



# **CENTER FOR INFRASTRUCTURE ENGINEERING STUDIES**

## **Blast Resistance of Un-reinforced Masonry Walls Retrofitted with Fiber Reinforced Polymers**

**by**

**Khaled A. El-Domiaty**

**Dr. John J. Myers**

**Dr. Abdeldjelil Belarbi**

**Department of Civil Engineering**

**University of Missouri - Rolla**

**CIES**

**02-24**

### **Disclaimer**

The contents of this report reflect the views of the author(s), who are responsible for the facts and the accuracy of information presented herein. This document is disseminated under the sponsorship of the Center for Infrastructure Engineering Studies (CIES), University of Missouri -Rolla, in the interest of information exchange. CIES assumes no liability for the contents or use thereof.

The mission of CIES is to provide leadership in research and education for solving society's problems affecting the nation's infrastructure systems. CIES is the primary conduit for communication among those on the UMR campus interested in infrastructure studies and provides coordination for collaborative efforts. CIES activities include interdisciplinary research and development with projects tailored to address needs of federal agencies, state agencies, and private industry as well as technology transfer and continuing/distance education to the engineering community and industry.

Center for Infrastructure Engineering Studies (CIES)  
University of Missouri-Rolla  
223 Engineering Research Laboratory  
1870 Miner Circle  
Rolla, MO 65409-070  
Tel: (573) 341-6223; fax -6215  
E-mail: [cies@umr.edu](mailto:cies@umr.edu)  
[www.cies.umr.edu](http://www.cies.umr.edu)

**COPYRIGHT 2002**

K. El-Domiaty, J.J. Myers, A. Belarbi

All Rights Reserved

## ABSTRACT

The increased amount of terrorist activities directed against U.S. facilities led to an evaluation of the survivability of masonry structures to blast loadings. Un-reinforced masonry (URM) walls have a low resistance against out-of-plane blast loading due to their low flexural capacity and their brittle mode of failure. Therefore, failures of URM walls were identified as one of the major causes of material damage and loss of human life due to blast loads. This led to an urgent need in developing effective retrofitting techniques instead of impractical conventional approaches to upgrade masonry members to resist blast loads. An alternative method is using Fiber Reinforced Polymer (FRP) composites on the surfaces of the walls to resist high flexural stresses. However, this is a new approach to blast resistant design and there is little available test data to use as a basis for design of wall upgrades.

Two series of walls, reflecting different slenderness ratios and strengthened with FRP composite materials were included in this research study by varying charge weights and standoff distances. FRP composites in the form of rods and laminates were used as strengthening materials. The walls were supported from the top and bottom and subjected to blasts from mid-height. The tests caused a well-distributed range of damage levels; from no damage to complete failure and the shear capacity controlled the blast behavior of the strengthened walls. Furthermore, the analytical analysis showed that the single degree of freedom (SDOF) approach can be used to predict the behavior of masonry walls strengthened with FRP. Conclusions and design guidelines relating deformation limits to threat and damage levels are provided with recommended future research needs.

## **ACKNOWLEDGMENTS**

This project was funded by the NSF Industry/University Cooperative Research Center on Repair of Buildings and Bridges with Composites located at the University of Missouri-Rolla (UMR). The authors wish to acknowledge this funding agency. In addition the authors would like to acknowledge the support received from the Center for Infrastructure Engineering Studies (CIES) as well as Dr. Paul Worsley and his associates in the Rock Mechanics and Explosives Research Center at UMR for their efforts in handling and setting off the explosive charges associated with the field blast tests.

## TABLE OF CONTENTS

	Page
ABSTRACT .....	iii
ACKNOWLEDGMENTS .....	iv
LIST OF ILLUSTRATIONS .....	vii
LIST OF TABLES .....	ix
1. INTRODUCTION .....	1
1.1. BACKGROUND .....	1
1.2. SCOPE AND OBJECTIVES .....	4
1.3. REPORT LAYOUT .....	6
2. LITTREATURE REVIEW .....	8
2.1. NATURE OF EXPLOSIONS .....	8
2.2. Retrofitting of Masonry Walls .....	13
2.2.1. Conventional Strengthening Methods .....	15
2.2.2. Strengthening with FRP Composites .....	17
3. FRP COMPOSITE SYSTEMS .....	22
3.1. MECHANICAL PROPERTIES .....	22
3.2. STRENGTHINING SCHEMES .....	24
3.2.1. Laminate Lay-up .....	24
3.2.2. Near Surface Mounted (NSM) Rods .....	26
3.2.3. Hybrid Systems .....	29
4. RESEARCH PROGRAM .....	30
4.1. EXPERIMENTAL DESIGN .....	30
4.2. TEST MATRIX .....	32
4.3. TEST SETUP .....	35
4.4. TESTING EQUIPMENT AND INSTRUMENTATION .....	37
5. PRESSURE ANALYSIS AND MODEL DEVELOPMENT .....	40
5.1. PRESSURE CALIBRATION .....	40
5.2. PRESSURE AND DEFLECTION WAVE RESULTS .....	41

5.3. MODEL DEVELOPMENT FOR PEAK PRESSURE DETERMINATION...	43
6. TEST RESULTS, DISCUSSION AND ANALYTICAL ANALYSIS .....	46
6.1. TEST RESULTS.....	46
6.1.1. Results of Series I - 4 in. CMU Walls.....	47
6.1.2. Results of Series II - 8 in. CMU Walls.....	56
6.1.2.1 Standoff Blast Phase .....	56
6.1.2.2 Surface Blast Phase.....	61
6.2. TEST DISCUSSION .....	64
6.2.1. Un-reinforced Masonry Walls Behavior .....	65
6.2.2. FRP Retrofitted Masonry Walls Behavior .....	66
6.2.2.1 FRP retrofitted masonry walls in series I.....	66
6.2.2.2 FRP retrofitted masonry walls in series II .....	69
6.2.2.2.1 Standoff blast phase .....	69
6.2.2.2.2 Surface blast phase.....	70
6.3. ANALYTICAL STUDY .....	71
6.3.1. Analysis Study for Un-reinforced Masonry Walls.....	77
6.3.2. Analysis Study for FRP Retrofitted Masonry Walls .....	80
7. CONCLUSIONS AND RECOMMENDATIONS FOR FUTURE RESEARCH .....	86
7.1. CONCLUSIONS.....	86
7.2. FUTURE RECOMMENDATIONS .....	87
APPENDICES	
A. PRESSURE AND DEFLECTION RESULTS .....	89
B. BLAST ANALYSIS; FACTORS, EQUATIONS AND REQUIREMENTS .....	98
C. SINGLE-DEGREE-OF-FREEDOM DETAILED ANALYSIS .....	104
BIBLIOGRAPHY.....	116



## LIST OF ILLUSTRATIONS

Figure	Page
1.1 Un-strengthened Masonry Wall after Blast Loading.....	5
1.2 URM Wall Strengthened with FRP after Blast Loading .....	5
2.1 Typical Blast Pressure Wave .....	10
2.2 Linearized Blast Pressure Wave .....	10
3.1 Installation of FRP Sheets (Tumialan 2001).....	25
3.2 Installation of Surface Mounted FRP Rods (Tumialan 2001) .....	26
3.3 FRP Structural Repointing (Tumialan 2001).....	27
3.4 Tuck Pointing of FRP Rods (Tumialan 2001) .....	28
3.5 Hybrid System including FRP Rods and Sheets.....	29
4.1 Construction of the Half Panel.....	33
4.2 Completion of the Whole Wall.....	33
4.3 Retrofitting Schemes.....	34
4.4 Test Setup for Blast Test of URM Walls .....	35
4.5 The Eight Walls Constructed and Prepared for Testing .....	36
4.6 Pressure Transducer Used in This Study .....	37
4.7 Pressure Transducer Placed at the Front Face of Wall .....	37
4.8 Accelerometer Placed to Back Face of Wall .....	38
4.9 Location of Transducers and Accelerometers Throughout the Wall .....	39
5.1 Typical Pressure Wave Profile.....	41
5.2 Typical Deflection Wave Profile .....	42
5.3 Peak Pressure vs. Charge Weight Relationship at 12 ft.....	43
5.4 Peak Pressure vs. Radial Distance Relationship at 1 lb .....	44
5.5 Experimental vs. Empirical Model Data.....	45
6.1 Wall U1 after Event #5 .....	48
6.2 Failure of Wall U1 after Event #6.....	48
6.3 Horizontal Crack in Epoxy Joint in Wall A1 after Event #5 .....	50
6.4 Shear Crack at Top Support of Wall A1 at Event #6.....	51

6.5 Cracks at Front Face of Wall A1 after Event #6.....	51
6.6 Shear Crack at Top Support of Wall B1 after Event #6 .....	53
6.7 Collapse Failure of Wall B1 after Event #7.....	53
6.8 Shear crack at Top Support of Wall C1 after Event #5 .....	55
6.9 Front Face of C1 after Event #6.....	56
6.10 Collapse of C1 after Event #7.....	56
6.11 Cracks of U2 after Event #5.....	58
6.12 Failure of U2 after Event #6 .....	58
6.13 Blow-up View after Event #6 .....	58
6.14 Wall U2 after Event #7 .....	58
6.15 Shear Failure after Event #6 .....	60
6.16 Horizontal Crack after Event #6 .....	60
6.17 Wall A2 after Event #6 .....	61
6.18 Collapse of A2 after Event #7.....	61
6.19 Front Side of U3 after Event #1 .....	62
6.20 Backside of U3 after Event #1 .....	62
6.21 Front Side of Wall C2 after Event #1 .....	63
6.22 Side View of C2 after Event #1 .....	63
6.23 Side View of C2 after Event #2 .....	63
6.24 Total Collapse of Wall C2 after Event #3.....	64
A.1.1 Pressure Wave vs. Time at 0.5 lb @ 16ft for Wall U1 at p3 .....	90
A.1.2 Pressure Wave vs. Time at 1.5 lb @ 12ft for Wall A1 at p2 .....	90
A.1.3 Pressure Wave vs. Time at 3.0 lb @ 12ft for Wall A1 at p2 .....	91
A.1.4 Mid-span Deflection Wave vs. Time at 0.5 lb @ 16ft for Wall B1 .....	91
A.1.5 Pressure Wave vs. Time at 1.0 lb @ 12ft for Wall C1 at p3.....	92
A.1.6 Pressure Wave vs. Time at 1.5 lb @ 12ft for Wall C1 at p3.....	92
A.1.7 Pressure Wave vs. Time at 1.5 lb @ 12ft for Wall C1 at p2.....	93
A.1.8 Pressure Wave vs. Time at 3.0 lb @ 12ft for Wall C1 at p2.....	93
A.1.9 Pressure Wave vs. Time at 1.0 lb @ 12ft for Wall U2 at p5 .....	94
A.1.10 Mid-span Deflection Wave vs. Time at 1.0 lb @ 12ft for Wall U2.....	94
B.2.1 Graphical Solution Chart for SDOF System.....	103

## LIST OF TABLES

Table	Page
2.1 Conversion Factors for Explosives .....	12
3.1 Resin Properties .....	23
3.2 FRP Properties .....	23
4.1 Levels of Damage to Tested Walls .....	31
4.2 Antiterrorism/Force Protection Design Parameters .....	31
4.3 Test Wall Matrix Retrofitting Schemes .....	34
5.1 Pressure Calibration Stage .....	40
5.2 Experimental and Theoretical Peak Pressure Values at Test Wall #4 (C1).....	43
6.1 Blast Events vs. Damage and Threat Levels Correlations of Wall U1 .....	47
6.2 Blast Events vs. Damage and Threat Levels Correlations of Wall A1 .....	49
6.3 Blast Events vs. Damage and Threat Levels Correlations of Wall B1 .....	52
6.4 Blast Events vs. Damage and Threat Levels Correlations of Wall C1 .....	54
6.5 Blast Events vs. Damage and Threat Levels Correlations of Wall U2.....	57
6.6 Blast Events vs. Damage and Threat Levels Correlations of Wall A2.....	59
6.7 SDOF Analysis Results for Wall U1 at Different Blast Events.....	78
6.8 SDOF Analysis Results for Wall U2 at Different Blast Events.....	79
6.9 SDOF Analysis Results for Wall B1 at Different Blast Events.....	82
6.10 Damage and Threat Levels vs. Rotation and Ductility Ratios for Wall B1 .....	84
6.11 Support Rotation Guidelines for FRP Strengthened Walls.....	85
6.12 Ductility Ratio Guidelines for FRP Strengthened Walls .....	85
A.2.1 Experimental and Theoretical Peak Pressure Values at Test Wall # 1 (U1).....	95
A.2.2 Experimental and Theoretical Peak Pressure Values at Test Wall # 2 (A1).....	95
A.2.3 Experimental and Theoretical Peak Pressure Values at Test Wall # 3 (B1).....	96
A.2.4 Experimental and Theoretical Peak Pressure Values at Test Wall # 4 (C1).....	96
A.2.5 Experimental and Theoretical Peak Pressure Values at Test Wall # 6 (U2).....	96
A.2.6 Experimental and Theoretical Peak Pressure Values at Test Wall # 7 (A2).....	97
B.1.1 Transformation Factors, for Simply Supported Members .....	99

B.1.2 Transformation Factors, for Fixed Supported Members .....	100
B.1.3 Transformation Factors, for Simple-Fixed Supported Members .....	101
B.2.1 Strength Increase Factors (SIF).....	102
B.2.2 Dynamic Increase Factors (DIF).....	102
B.2.3 Deformation Limits for Masonry .....	103

# **1. INTRODUCTION**

## **1.1. BACKGROUND**

Modern terrorism is one of the major threats to United States facilities, interests and personnel throughout the world. It is described as the deliberate use of violence to create a sense of shock, fear, and outrage in the minds of a target population. In the past eight years, the United States and its citizens have been the victims of major bombing attacks. The attack on the World Trade Center in New York City in February 1993 and on the Alfred P. Murrah Federal Building in Oklahoma City in April 1995 occurred on U.S. land. Attacks outside the country included bombing of the military complex in Dhahran, Saudi Arabia, in 1996 and the bombings of the U.S. embassies in Kenya and Tanzania in 1998. In the year 2001, attacks on the World Trade Center in New York City and the Pentagon in Virginia leading to catastrophic loss in lives and property, have illustrated the recent escalation in terrorist attacks and its direct impact on the social and economical stability of this nation and other nations worldwide.

Although these events have generated a wide knowledge of the consequence of terrorism, many public, federal and corporate buildings and installations have been built and are still being built with minimal or no concern for the destructive effects of terrorist attacks. This raises a considerable concern about the ability of the government to protect buildings and their occupants from bombings and other direct physical attacks.

Due to the increased amount of terrorist activities directed against U.S. facilities, both civil and military, evaluation of the survivability of masonry structures to blast loadings was needed. Masonry buildings exist in large numbers worldwide, and incorporate approximately 70% of the existing building inventory in the United States.

Most of these buildings that were constructed of un-reinforced masonry (URM) are used for public, federal or commercial uses. Typically, these structures have high occupancy levels and are not designed to resist air blast loadings from high explosives.

Protection of these buildings and their inhabitants can consume vast amounts of resources and yet never offer a guarantee of safety. Determining an acceptable level of protection is also a concern because the magnitude of risk varies. Some loss of property may be acceptable, but certain losses such as essential records, specialized equipment, or human life are catastrophic. Risk assessments are necessary to optimize the design of structures with regard to counteracting terrorist attacks. Some level of risk can be tolerated for some structures, while other structures must be protected at all costs.

In addition, the location and type of structure are important in a risk assessment analysis. Certain countries and certain regions within a particular country, and particular types of buildings (such as government or military buildings) are more susceptible to attacks. These factors play a great role in determining risk analysis and the need for protection against those attacks.

When designing structural elements in accordance with local, state, and industry regulations, safety factors are applied to loads and strengths of material components. In designing against blast loading, there are several additional conditions that may apply:

- The incident will be an unusual event.
- The threat will be specified in terms of an explosive charge weight at a distance (called the standoff), which can only be an estimate and already subject to a risk assessment.

- For economic design, some plastic deformation is normally permitted. The level of damage is specified in terms of the limiting member deflection or support rotations.
- The strengths of the materials will be enhanced because of the high rate of strain to which they will be subjected.
- The strengths of in-situ materials often exceed the characteristic values.

Because of these factors, designers must carefully evaluate all aspects of the design with regard to potential blast loadings. This is a difficult task, yet several design philosophies are available to address it. It is also important to note that prior to structural considerations of design, substantial planning can aid in deterring attacks before they happen. Building layout, security, disguise of entrances and other physical barriers are important tools in preventing attack.

After a threat or risk analysis is complete, one can estimate the size and location of the explosion to protect against. By using the relationship that the intensity of a blast decays in relation to the distance from the explosion, one can adopt an idealized blast wave at the target. Using published data the characteristics of that blast wave can be determined.

The mechanics of an explosion must be understood before explosion data can be analyzed or predicted. An explosion is a very fast chemical reaction producing transient air pressure waves. For a ground-level explosive device (such as a bomb in a vehicle), the pressure wave will travel away from the source in the form of a hemispherical wave front if there are no obstructions in its path. The peak overpressure (the pressure above normal atmospheric pressure) and the duration of the overpressure vary with distance from the

device. The magnitude of these parameters also depends on the explosive materials from which the bomb is made and the packaging method for the bomb. Usually the size of the bomb is given in terms of an equivalent weight in Trinitrotoluene (TNT). Methods exist for the design of structural elements subjected to blast loads from bombs of specified charge weights.

It is impossible to predict with great accuracy the size or effects of a bomb explosion on any particular building. Designers should attempt to form an opinion about the possible threats and likely effects of such threats.

As mentioned previously, the standoff distance (the distance between the bomb and the structure) is a fundamental parameter when determining the blast pressures experienced by a building. As standoff distance increases, blast pressure drops significantly. For a device placed inside a building (the stand-off distance being now effectively zero), greater damage and more injuries would be caused than if the same sized device were deployed outside the building.

## **1.2. SCOPE AND OBJECTIVES**

Previous research (as described later in the Literature Review Section) has demonstrated that the capacity and ductility of masonry walls subjected to blast loads can be increased by means of FRP composites. The University of Missouri-Rolla (UMR)/Center for Infrastructure Engineering Studies (CIES) has developed a comprehensive program to assess the feasibility of using FRP composite materials to upgrade the blast resistance of masonry walls. A preliminary pilot study (conducted prior to this research program) demonstrated effectiveness of FRP composites. For two masonry walls



subjected to the same blast load located at the same standoff distance, the un-strengthened wall collapsed due to the explosive wave, illustrated in Figure 1.1. Exterior and interior face damage is illustrated in Figure 1.1-a and b. Conversely, the wall strengthened with FRP laminates suffered minor damage (see Figure 1.2). As shown from Figure 1.2-a and b, the retrofitted wall was also able to withstand higher blast loads.



(a) Exterior Face



(b) Interior Face

Figure 1.1 Un-strengthened Masonry Wall after Blast Loading



(a) Exterior Face



(b) Interior Face

Figure 1.2 URM Wall Strengthened with FRP after Blast Loading

The main objective of this project is to demonstrate the performance and implementation of this new technology (application of FRP) for the protection of existing and new masonry buildings against blast loads as an alternative to traditional concrete or steel retrofit techniques with a view to provide blast resistant design/retrofit guidelines for counteracting terrorist attacks.

There are two other specific purposes in this research program. The first one is predicting peak pressure values resulting from an explosion at a given charge weight and standoff distance while the other purpose is to predict the dynamic response of the URM walls strengthened with FRP using simplified dynamic analysis procedures that are commonly used in determining the response of structural components to blast loads.

### **1.3. REPORT LAYOUT**

This dissertation is organized for the development of the investigation according to the following stages. Chapter one introduces the importance of the strengthening of masonry elements due to the increased amount of terrorist activities directed against the United States, which led to setting up the objectives of this research. Chapter two goes through a review on the nature of explosives and theoretical models for predicting blast pressure. Chapter two also goes through a review on the strengthening approaches used for URM walls using conventional and FRP materials strengthening methods to withstand blast loads. FRP material properties and strengthening schemes are introduced in Chapter three. Chapter four gives a detailed description of the research program including the experimental design, test matrix and setup and the measuring instrumentation used through out this research. In Chapter five, experimental pressure and deflection profiles gained from the test instrumentation were validated with the

theoretical pressure models and used to develop a model to determine peak pressure values at a given charge and standoff distance. Test results and observations with a detailed discussion are presented in Chapter six. An analytical study for the behavior the URM walls strengthened with FRP using a single degree of freedom approach is also presented in chapter six. Finally, chapter seven provides conclusions, design guidelines and future recommendations in the area of strengthening URM walls with FRP to resist blast loads.

## 2. LITTREATURE REVIEW

### 2.1. NATURE OF EXPLOSIONS

Explosions can be classified as physical, nuclear, or chemical explosions. A chemical explosion usually involves the rapid oxidation of fuel elements (carbon and hydrogen atoms) forming part of the explosive compound. The rate of reaction will determine the usefulness of the explosive material for practical applications.

Most common explosives are either solids or liquids, called “condensed”. When the explosive begins to react it decomposes violently with the evolution of heat and the production of gas. The rapid expansion of this gas results in the generation of shock pressures in any solid material with which the explosive is in contact or blast waves if the expansion occurs in air. “Fuel-air” or “vapor cloud” explosions are less commonly used by terrorists, but can produce damage to structures equal or greater to that produced by condensed high explosives. These types of reactions generally produce lower pressures than an equivalent quantity of condensed explosives, but may endure for a longer period of time.

High explosives detonate to create shock waves, burst or shatter materials in or on which they are located, penetrate materials, produce lift and heave of materials and, when detonated in air or under water, produce air-blast or underwater pressure pulses. Low explosives detonate to produce pressure pulses generally of smaller amplitude and longer duration than high explosives—an example of low explosives are mixtures used to make gunpowder.

Explosives can also be classified as primary or secondary, depending on how they are initiated. Primary explosives are those that can be easily initiated by spark, flame or

impact. Examples of this include mercury fulminate and lead azide. Secondary explosives can be initiated less easily than can primary explosives. Examples include TNT and RDX (also known as cyclonite). It is common practice for both military and commercial explosive manufacturers to blend explosive compounds. For commercial use, explosives are generally made from less expensive materials. For example, nitroglycerine is mixed with low-cost nitrates. Military explosives are composed of more expensive materials such as mixtures of industry stable explosive compounds like TNT and RDX with TNT. These generally have a longer shelf life than commercial explosives.

Terrorist organizations typically have limited quantities of military-style high explosives such as Semtex. Often they manufacture their own explosives using farm fertilizer, for example. These types of explosives behave as detonating high explosive material.

The violent release of energy from a detonation in a gaseous medium gives rise to a sudden pressure increase in that medium. The pressure disturbance, termed as the blast wave, is characterized by an instantaneous rise from the ambient pressure,  $P_o$ , to peak incident pressure  $P_{so}$ . At a point away from the blast, the pressure wave has almost a triangular shape as shown in Figure 2.1.

The shock front arrives and after the rise to the peak value the incident pressure decays to an ambient value in the time,  $t_d$ , described as the positive phase duration. This is followed by a negative phase,  $t_{ng}$ , and characterized by a pressure below the pre-shot ambient pressure and a reversal of the particle flow. The negative phase is usually less important in a design than the positive phase. The incident impulse associated with the blast wave is the integrated area under the pressure time curve and is denoted as  $I_{so}$ . To

simplify the blast resistant design procedure, the generalized blast wave profile shown in Figure 2.1 is usually linearized as illustrated in Figure 2.2.

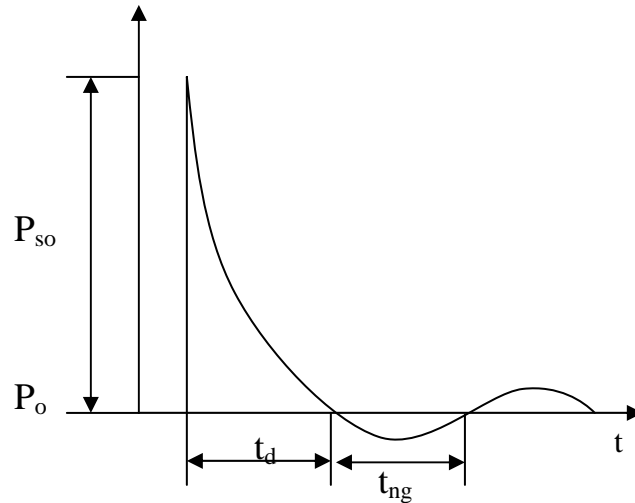


Figure 2.1 Typical Blast Pressure Wave

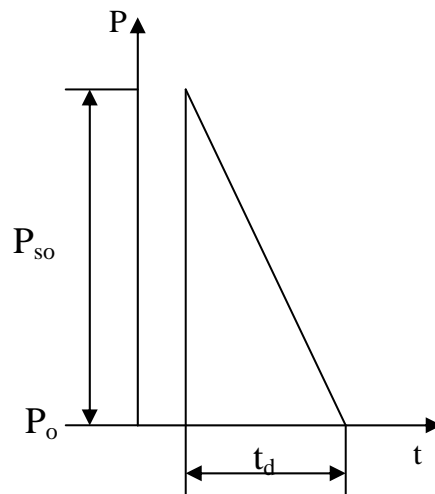


Figure 2.2 Linearized Blast Pressure Wave

The explosion in air results in a shock wave that propagates spherically away from the center of the explosion. As mentioned briefly in the previous chapter, two main parameters describe the blast wave pressure. The charge weight,  $Q$ , is the weight of

explosive in pounds or kilograms is the first parameter. The second parameter is the standoff distance,  $R$ , which is the radial distance from the center of the explosive to a particular location on a structure, measured in feet or meters.

Extensive research has been conducted to predict the peak pressure values, impulse velocities and other parameters of blast waves. Most of the theoretical models and graphs were done by military research centers, in which they correlate between a scaled distance  $Z [= R/(Q^{1/3})]$  and the predicted peak pressures. Two models were used in this research program to predict peak pressure values to compare them to the measured pressure values. The first model was based on an empirical equation presented by Charles N. Kingery and Gerald Bulmash and reflected pressure coefficients listed in the United States Army technical manual TM5-855-1. This equation computed air blast environment created by the detonation of a hemispherical TNT explosive source at sea level. Information on this model is classified and therefore cannot be introduced in this discussion. From herein this relationship will be referred to as Model 1 within the discussion of this report. The second model is based on an empirical equation presented by the Defense Atomic Support Agency, DASA report # 1860 (1966). This equation correlates between the peak pressure with the weight and standoff distance as shown in equation 2.1 below and referred to as Model 2.

$$P_{so} = 150Q(5/R)^3 \text{ where,} \quad (\text{Equation 2.1})$$

$P_{so}$ : Peak pressure at given charge weight and standoff distance in psi

$Q$ : Charge weight of TNT in pounds

$R$ : Radial standoff distance from the center of the explosive to a particular location on a structure, measured in feet

TNT is used as the “reference” explosive in forming empirical equations. Therefore, first stage in quantifying blast waves from sources other than TNT is to convert the actual mass of the charge into a TNT equivalent mass. The simplest way to do this is to multiply the mass of explosive by a conversion factor based on its specific energy and that of TNT. Conversion factors for a number of common explosives are given in Table 2.1, adapted from Baker et al., (1983).

Table 2.1 Conversion Factors for Explosives

<b>Explosive</b>	<b>Mass Specific Energy <math>Q_x</math> (kJ/kg)*</b>	<b>TNT Equivalent <math>Q_x/Q_{TNT}</math></b>
Compound B (60% RDX, 40% TNT)	5190	1.148
RDX (Cyclonite)	5360	1.185
HMX	5680	1.256
Nitroglycerin (liquid)	6700	1.481
TNT	4520	1.000
Pentolite	6012	1.330
60% Nitroglycerin dynamite	2710	0.600
Semtex	5660	1.250

\* Convert to (Btu/lb) by multiplying by 0.43

The TNT equivalence of terrorist-manufactured explosive material is difficult to define precisely because of the variability of its formulation and the quality of the control used in its manufacture. TNT-equivalent factors ranging from as low as 0.4 (for poor quality explosives) up to almost unity have been suggested. Similarly for fuel-air or vapor



cloud explosives, TNT equivalence is difficult to specify accurately. A factor of between 0.4 and 0.6 is sometimes used.

## **2.2. RETROFITTING OF MASONRY WALLS**

Explosives have been used for hundreds of years, yet comprehensive treatment of blast effects and their mitigation appeared in the Western Hemisphere only during and after World War II, where, a lot of development was done on imploding damaged structures learning the affect of structures to near field explosions. In the United States, the accelerated arms race during the Cold War, from 1945 through 1990, led to extensive research in order to increase the blast resistance of military structures. Much of this research was in response to deployment of ballistic and guided missile systems that developed manuals for military protective structures. These manuals concentrated on techniques for estimating the loadings from nuclear and conventional weapons and explosions, attenuation of pressure effects in the air and ground, guidelines for designing and analyzing equipment and other related topics.

Ending the Cold War and entering the 1990's, the United States faced a different kind of terrorism that targeted commercial, civilian and governmental buildings. These attacks have made it so abundantly clear that the United States is vulnerable to a continuing threat of terrorist bombing. The awareness of this threat by both policy makers and the general public facilitated acceptance of the desirability and timeliness of transfer and application of some military protective technologies to civilian structures. This led to extensive research in order to increase the blast resistance of commercial and civilian structures.

But, designing and upgrading civilian or commercial buildings to withstand the effects of a terrorist blast was unlike the design of military structures. Military structures are typically associated with a specific mission that must be maintained, and they must remain operational despite the attack. They occupy secure sites with substantial restricted barrier distances surrounding the assets; unfortunately, this is not possible for most civilian structures. Civilian owners typically want to attract the public to keep the property profitable and can rarely afford the real estate necessary to secure the site. The restricted barrier distance is vital in the design of blast resistant structures since it is the key parameter that determines, for a given charge weight, the blast pressures that load the building and its structural elements. The degree of fenestration is another key parameter as it determines the pressures that enter the structure. The smaller and fewer doors and window openings are, the better the occupants are protected within the structure. Following these key parameters, architectural and structural features play a significant role in determining how the building will respond to the blast loading.

Hence, the role of civil and blast engineers was further complicated by structural and architectural criteria that directly contradicted the blast-mitigation objectives using military protective technologies. The objectives were therefore more modestly defined to permit significant localized damage while preventing catastrophic collapse to save lives and evacuate victims. Therefore, new means and technologies were needed to achieve these new objectives. Attention was given to the design and behavior of the structural elements to improve their redundancy, toughness and ductility to resist blast loads. Infill un-reinforced masonry walls; one of the structural elements of a building; was chosen to be upgraded in this research program.

Most of the exterior walls of civilian and commercial structures through out the United States are constructed of un-reinforced concrete masonry units. These infill URM walls have a low resistance against lateral, out of plane blast loading. The low capacity is due to low flexural strength and the brittle mode of wall failure. An explosive charge detonating close to a building may result in the breakup of the exterior URM walls. Wall debris resulting from the blast, potentially at high velocity, is a significant hazard and a leading cause of injury and death to building occupants. The response of URM walls is dependent on the weight, location and type of explosives, as well as the wall type and structural geometry. Therefore, hazard levels to the building occupants were defined (described in Section 4.1) and achieved throughout the proposed experimental program.

Since there are many existing masonry buildings, it is understandable that buildings owners would be interested in a solution to protect all these types of buildings. Throughout the past 10 years there has been several techniques and attempts to harden existing structures against blast effects. Because of the high cost of these existing retrofitting methods, developing improved and convenient methods and technologies are needed. One of these latest technologies entering the market is applying FRP composites to strengthen existing un-reinforced masonry walls. Therefore, retrofitting methods of masonry structures have been classified in this research into two methods; conventional methods and strengthening with FRP Composites.

**2.2.1. Conventional Strengthening Methods:** Upgrading civilian or commercial buildings to withstand the effects of a terrorist blast is unlike the design of military structures due to architectural and structural limitations. That led engineers to impractical structurally upgraded techniques for the structural elements of the buildings. Un-

reinforced infill masonry walls (one of these structural elements) have been strengthened using the following techniques:

- Additional mass: by increasing the walls thickness to enhance their stability.
- Additional strength: by modification of boundary conditions, reduction in loaded area, adding steel reinforcement or steel plates and structures.
- Replacement of weak components: by removing un-reinforced masonry walls and installing blast resistant reinforced walls.

However, these techniques result in limitations that may present additional problems. Adding mass to a building component has an effect where damage is caused by impulsive loading while loading from explosives is dynamic in nature. Also, the addition of mass contributes to the weight of the building, which often places greater demands on the existing framing and foundations. It is usually difficult and expensive to add additional foundation capacity. It also results in structures that are more susceptible to earthquake damage in seismic regions.

Adding strength and stiffness to the structure are also challenging. Such approaches usually require additional walls and columns that are not suitable for long span structures. Also, another solution dealing with reduction of loaded areas that refers to earth beams placed against exterior walls of the building has possibilities depending on the site conditions and the exterior wall material, but it is certainly not a broad-based solution. Modifying boundary conditions also has its limitations, especially dealing with infill masonry walls. Also, adding steel reinforcement or steel panels to restrain the wall can be either impractical or require significant labor during installation, especially for

walls with many openings. Steel structures also need special attention where they are employed to resist blast loading since they will often respond in an inelastic manner to blast loading. Of particular concern are the connections. If the connections fail, it can lead to instability of the structure and possibly collapse.

Replacing URM walls with new blast resistant walls is another technique used for retrofitting structures. This technique is often impractical based upon the layout and structural system of the structure. It also often requires significant labor and time that is not cost effective.

**2.2.2. Strengthening with FRP Composites:** The conventional methods mentioned above for retrofitting URM walls face either impracticality or high cost and time constraints for installation. Therefore, new technologies were implemented to harden masonry walls against blast loads such as strengthening with FRP composites. There have been several research studies on using FRP to retrofit un-reinforced masonry walls against out-of-plane blast loads. These are described below.

Muszynski, L.C. (1998) investigated three masonry walls that were subjected to two high explosive detonations. Two walls were built without reinforcement and one was retrofitted with CFRP laminates that were bonded to the surface. The masonry walls had nominal dimensions of 9.22 ft × 8.53 ft × 0.66 ft (2.81 m × 2.60 m × 0.20 m) and were constructed within a reinforced concrete frame with lightweight masonry blocks. The lightweight masonry sandstone blocks had a nominal size of 7.87 in. × 7.87 in. × 19.69 in. (200 mm × 200 mm × 500 mm). They had a compressive strength of 362.2 psi (2.5 MPa) and a unit weight of 33.71 pcf (540 kg/m<sup>3</sup>). The CFRP sheets had a thickness of

0.02 in. (0.5 mm) with a fiber orientation of 0/90/0. The sheets had a tensile strength of 329 ksi (2.27 GPa) and a modulus of 20 Msi (138 GPa).

The masonry walls were tested at various standoff distances. The first wall, unreinforced, was tested at a standoff distance of 95 ft (29 m). The second wall, reinforced with CFRP, was tested at the same standoff distance of 95 ft (29 m). The third wall, unreinforced, was tested at a standoff distance of 88.6 ft (27 m).

The first un-reinforced wall suffered a 7.48 in. (190 mm) displacement at the mid-height. Spalling of the front face occurred throughout the masonry section. All mortar joints had failed. An arch formed between the two center blocks and prevented the wall from breaching. The second wall retrofitted with CFRP had a considerable spalling on the front face and all mortar joints were broken. The backside measured 0.12 in. (3 mm) residual displacement at the mid-height and the CFRP felt loose to the touch because the masonry block was pulverized. The third un-reinforced wall breached and the concrete frame moved 1.97 in. (50 mm).

It was concluded from this research that the CFRP reinforced walls were damaged due to delamination of the composite material and the CFRP failed in tension at the mid-wall height. It is also concluded that the CFRP strengthened walls had a less residual displacement than the bare control walls.

Baylot (2000) conducted experiments on concrete masonry unit (CMU) walls using 1/4 scale models of typical 8 in. (203 mm) wide CMU. The walls were reported as 15 blocks tall and 15.5 blocks wide and were constructed within a frame (infill walls) that was attached to a reaction frame. The three wall series were un-grouted (Series A), fully grouted (Series B) and partially grouted (Series C). In the partially grouted walls every

third vertical cell was filled with grout. In the fully grouted walls, all cells were grouted full height.

Three types of retrofits were evaluated for Series A and C. The first retrofit method consisted of 0.04 in. (1 mm) thick E-GFRP fabric bonded to the back face of the wall. The laminate had a modulus of elasticity of 3.79 Msi (26.13 GPa), a tensile strength of 87 ksi (600 MPa), a 2.24% elongation at break and a mass density of 0.06 pcf (0.92 kg/m<sup>3</sup>). The second retrofit technique consisted of a two-part sprayed-on polyurea applied to the back face of the wall. The approximate thickness of the material was 0.13 in. (3.2mm). The material has a modulus of elasticity of 34 ksi (234 MPa), secant modulus of 24 ksi (165 MPa), yield strength of 1,668 psi (11.5 MPa) and ultimate strength of 2,000 psi (13.8 MPa). In the third type of retrofit, 20-gage [0.04 in. (1mm) thick] hot-dipped galvanized A-36 ksi (248 MPa) steel sheet metal was attached behind the wall.

For the un-grouted walls (Series A), each of the three retrofit types was tested at the same level that caused the non-retrofitted wall to fail at a higher hazardous velocity. The CMU wall failed in each of the three retrofit experiments. But the FRP and polyurea retrofits prevented debris from entering the structure and were therefore considered successful retrofits. While, in the sheet metal retrofit the connections failed and resulted in a minor level of debris within the structure.

For the fully grouted walls (Series B), only un-reinforced walls were tested. These walls failed in larger sections and required more blast impulse than the un-grouted walls to fail due to the slight increase in strength and mass. Ultimately, the fully grouted walls failed at high velocities and debris entered the structure.

For the partially grouted walls (Series C), the retrofits focused the debris downward such the majority of the debris landed near the front of the structure. Therefore the retrofit techniques were successful in terms of reducing the hazard level inside.

Oswald and Chang (2001) performed twenty-one shock tube tests on ten unreinforced concrete masonry unit (CMU) walls that were strengthened with unidirectional Kevlar. These mats of Kevlar® fibers were attached with epoxy to both faces of walls. The test walls included walls with grouted and un-grouted voids, walls with and without openings, and walls with supports on two opposite sides and on all four sides.

The laminate had a Young's modulus of 6,000 ksi (41,370 MPa), a tensile strength of 110 ksi (758.4 MPa), a compressive failure strain of 0.0035 and a tensile failure strain of 0.018. The test walls were constructed from nominal 8 in (203.2 mm) thick lightweight CMU blocks. The blocks had an average Young's modulus of 2,000 ksi (13,790 MPa) and a tensile strength of 75 psi (517.1 kPa). The walls heights and widths were 100.5 in. (2.55 m) and 100 in. (2.54 m), respectively. Seven of the ten walls were supported top and bottom (one-way edge supported) and the other three walls were supported on all four sides (two-way edge supported). Kevlar mats were placed with the fibers oriented parallel to the direction of the wall span between supports.

A wide distribution of damage levels was observed, from no damage to complete failure. A significant number of walls exhibited both shear and flexural damage. Results from the tests showed that the grouted walls strengthened with Kevlar® had approximately 5 to 10 times more blast capacity than a corresponding un-strengthened wall. The blast capacities of walls without openings were controlled by shear strength and the blast capacities of walls with openings were controlled by flexural capacity. It was



noted that strengthened walls can resist higher pressures from blast loads with shorter durations. Oswald and Chang concluded that the blast capacity of un-grouted walls would typically be limited by the wall shear capacity, but a significant upgrade can still be achieved using Kevlar® reinforcement.

They also related between the ductility ratios (a ratio between the maximum to elastic deflection) of the walls to the damage levels for brittle responses of concrete as illustrated in Equation 2.1. Expected ductility ratios for a failure of concrete in shear or compression range from 1.3 to 1.9 in number of published criteria including ASCE (1997), Dark (1989) and ACI (1990). The value of 1.5 in Equation 2.1 is an average and is based on the assumption that brittle failure of the concrete masonry blocks would be similar to that of concrete. A ductility ratio of 1.0 is the upper bound of elastic response, where there is no damage expected in the elastic region.

$\mu < 1.0$	No Damage	(Equation 2.1)
$1.0 \leq \mu < 1.5$	Light or Heavy Damage	
$\mu \geq 1.5$	Failure	

where,

$\mu$  = ductility ratio of the wall defined as: maximum displacement of the member divided by its elastic limit displacement.

### 3. FRP COMPOSITE SYSTEMS

#### 3.1. MECHANICAL PROPERTIES

The most important characteristics of a strengthening project are the predominance of labor and shutdown costs as opposed to material costs, time, site constraints and long-term durability. The advantages of FRP versus conventional steel as a retrofitting material include lower installation costs, improved corrosion resistance, on-site flexibility of use, and minimum changes in the member size after repair. FRP material systems, which are composed of fibers embedded in an epoxy matrix, exhibit several properties suitable for their use as structural reinforcement. FRP composites are corrosion-resistant and non-conductive. Common FRP systems used in civil engineering infrastructure consist of fiber sheets and rods. These systems were used throughout this research study to investigate their effectiveness against blast loads. Two applications were investigated including externally bonded laminates where the sheets are attached to the member surface to form a composite laminate; and near surface mounted rods, where the rods are mounted in bed joints between courses near the surface.

For the externally bonded FRP sheets, the system consisted of three main materials: primer, putty and saturant. The combination of these materials with the fibers forms the FRP laminate. For near surface mounted rods, the system consisted of two materials: the epoxy-based paste and the rods. The properties for primer, putty, saturant and the epoxy-based paste are illustrated in Table 3.1 as given by the manufacturer.

To apply the appropriate retrofitting scheme for un-reinforced masonry walls, an appropriate retrofitted polymer material should be selected to be compatible with the low strength and stiffness of URM walls. Therefore, Glass Fiber Reinforced Polymers

(GFRP) is preferred because of their lower strength and stiffness than other materials like carbon and aramid. They are also less expensive than these other materials. GFRP sheets were selected for the study as well as GFRP rods. These were the only two FRP materials used to strengthen the masonry walls throughout this project. Their engineering properties according to the manufacturers are summarized in Table 3.2.

Table 3.1 Resin Properties

<b>Material</b>	<b>Tensile Strength (ksi*)</b>	<b>Tensile Elastic Modulus (ksi*)</b>	<b>Tensile Strain (%)</b>	<b>Compressive Strength (ksi*)</b>	<b>Compressive Modulus (ksi*)</b>
Primer	2.1	104	4.0	3.8	97
Putty	1.9	260	2.0	3.3	156
Saturant	7.8	440	2.5	12.5	380
Paste	4.0	NA	1.0	12.5	450

\* Converting to MPa, multiply by 6.89

Table 3.2 FRP Properties

<b>Material</b>	<b>Tensile Strength (ksi*)</b>	<b>Tensile Modulus (ksi*)</b>	<b>Load per Sheet Width (lb/in**)</b>
GFRP- EG900	240	12000	3050
#2 GFRP Rods	150	5200	-----

\* Converting to MPa, multiply by 6.89

\*\* Converting to N/m, multiply by 175.2

### 3.2. STRENGTHENING SCHEMES

The strengthening of masonry walls consisted of applying GFRP fibers by an epoxy resin matrix, as well as the installation of near surface mounted glass rods. Since the performance of the composite materials relies on bonding, installation procedures recommended by the manufacturers were important to follow and are as follows:

**3.2.1. Laminate Lay-up:** The FRP sheets are attached to the wall surface by manual lay-up. For their installation a procedure recommended by the manufacturer is followed. For concrete masonry, there is no need to sandblast the surface. Just leveling the surface with putty is enough for surface preparation. The dust resulting from grinding must be removed from the wall surface using air pressure to avoid potential bonding problems. The installation of the FRP sheets can be summarized as follows (See Figure 3.1):

- The primary purpose of using putty is to level the uneven surfaces present on the wall surface, especially at the mortar joints. After the putty has set, the surface is smoothed to eliminate irregularities on the surface. This task is carried out using a grinder (see Figure 3.1-a)
- Then, applied primer is to fill micro-cavities on the masonry wall surface. Due to the high rate of initial absorption of masonry units, some manufacturers recommend to apply the saturant used for impregnating the fibers as a primer. The constituent parts of the saturant usually have some particles settled on the bottom of the recipient; therefore, they are premixed independently.

- A layer of saturant is applied to the surface using a roller (see Figure 3.1-b). Following this, the FRP sheets are adhered to the wall surface (see Figure 3.1-c).
- Once, the sheet is placed, it is pressed down using a “bubble roller”, which eliminates the entrapped air between the saturant and fibers (see Figure 3.1-d). Finally, a second layer of saturant is applied.



(a) Leveling of Surface



(b) First coat of Saturant



(c) Installation of Fibers



(d) Entrapped Air elimination

Figure 3.1 Installation of FRP Sheets (Tumialan 2001)

**3.2.2. Near Surface Mounted (NSM) Rods:** The use of NSM rods is attractive since the removal of surface related activities are not required. For the walls where NSM rods are to be installed, the procedure can be summarized as follows (see Figure 3.2):

- Lines of 0.75 in (19.1 mm) wide are drawn on the wall at the desired location as guidelines for the specified width of the grooves.
- By using a grinder with a diamond blade, slots are then grooved, as illustrated in Figure 3.2-a. The masonry material is then removed using chisel and hammer to complete the slots. The depth of the groove depends on the wall thickness. The dust resulted from grooving is removed by air pressure.
- An epoxy-based paste is used to provide bond between the masonry and the rods. First, using a mason trowel, a layer of paste is placed into the slots. Following this, an FRP rod is nested in the slot (see Figure 3.2-b). The slot is then completely filled with the paste to encapsulate the FRP rod.



(a) Grooving of Slots



(b) NSM Rod Nested in the Paste

Figure 3.2 Installation of Surface Mounted FRP Rods (Tumialan 2001)

When the FRP rods are installed in either the horizontal or vertical (only for stack bond patterns) masonry joints, the aforementioned technique receives the name of FRP Structural Repointing. This is a traditional retrofitting technique, commonly used in the masonry industry, which consists in replacing missing mortar in the joints. The term “structural” is added to describe a strengthening method aimed at restoring the integrity and/or upgrading the capacity of walls. This is achieved by placing into the joints deformed FRP rods, which are bonded to the masonry wall by an epoxy-based paste (see Figure 3.3).

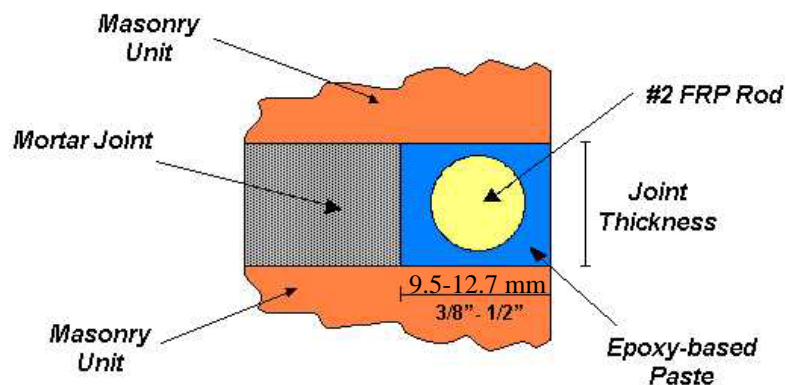


Figure 3.3 FRP Structural Repointing (Tumialan 2001)

The diameter size of the FRP rods is limited by the thickness of the mortar joint, which usually cannot be larger than 0.375 in (9.53 mm). The FRP rods are placed into the joints by using a technique known as tuck pointing, which consists of (see Figure 3.4):

- Cutting out part of the mortar using a grinder, the depth of the cut depends on the shell thickness of the masonry unit (see Figure 3.4-a). To ensure a proper bonding between the epoxy-based paste and masonry, it is recommendable to remove the dust by air pressure, once the grinding of the mortar joints has been completed.

- Masking of the masonry surface to avoid staining with the epoxy-based paste (see Figure 3.4-b).
- Filling the joints with an epoxy-based paste (see Figure 3.4-c).
- Embedding the rods in the joint (see Figure 3.4-d).
- Filling the rest of the space in the joints with the epoxy till the surface of the wall assuring proper bond and smooth surface.



(a) Grinding of Joints



(b) Masking of Masonry



(c) Application of Paste



(d) Installation of GFRP Rods

Figure 3.4 Tuck Pointing of FRP Rods (Tumialan 2001)



**3.2.3. Hybrid Systems:** For the hybrid system investigated within the research program, both FRP sheets and FRP rods were used to retrofit two masonry walls. First, installation of the FRP rods was done according to the procedures described previously, and then the surface was leveled with putty. After that, application of the FRP sheets was done using the procedures also described previously (See Figure 3.5).

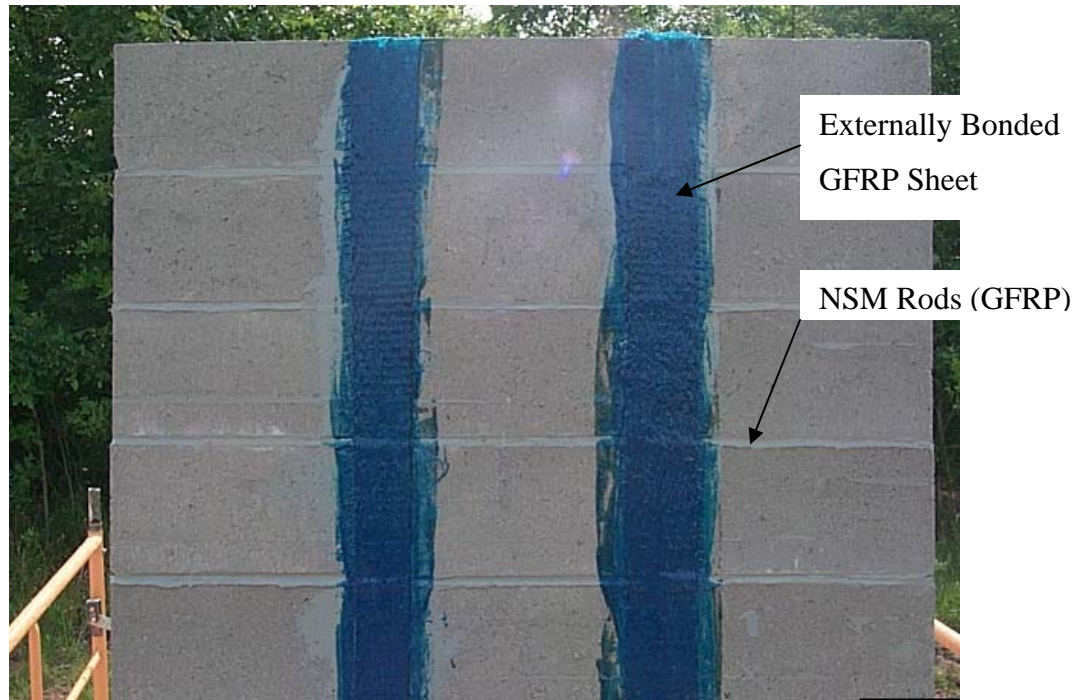


Figure 3.5 Hybrid System including FRP Rods and Sheets

## **4. RESEARCH PROGRAM**

### **4.1. EXPERIMENTAL DESIGN**

In order to obtain experimental data concerning blast loading and the associated effects on structures, significant research was carried out to determine the relationship between the nature of the blast loading (explosion) and the response of the tested masonry wall. Two main parameters are fundamental in determining the blast pressures experienced by a structure. These parameters included the charge weight,  $Q$ , and the standoff distance,  $R$ . The charge weight is the actual explosive material itself expressed in terms of mass, commonly in units of pounds. The standoff distance is defined as the distance between the explosive charge and the structure under loading, in this case the masonry walls.

In addition, the damage that occurred to the masonry walls as a result of the blast loading could be measured and correlated to the original two parameters. This correlation would indicate key relationships and provide insight for conducting risk assessment and determining acceptable levels of protection for walls under such blast loadings. As a good assessment tool, four levels of damage were picked to serve as hazard levels to be achieved during the experimental program as recommended by Interim Department of Defense (DOD) Anti-terrorism/Force Protection Construction Standards. Table 4.1 illustrates these damage levels for the tested walls, while Table 4.2 lists the anti-terrorism/force protection design parameters at different threat levels. A minimum threat level with no damage to the structure is required for design purposes. It is the purpose of this research to correlate such data for both un-reinforced masonry walls and walls strengthened by means of FRP.

Table 4.1 Levels of Damage to Tested Walls

<b>Level</b>	<b>Damage Level</b>	<b>Damage Description</b>	<b>Performance Description</b>
I	Failure	Wall falls out of test frame.	Wall crumbles and scattered debris.
II	Heavy Damage	Damage that definitely affects load capacity of wall. Wall will not survive same blast load.	Visible wide-open cracks or significant shear cracks, and damage to FRP retrofit. Small debris close to the wall.
III	Light Damage	Damage that does not affect load capacity but additional damage will be observed under same blast load.	Hairline to wider cracks at mortar joints or hairline shear cracks.
IV	No Damage	No damage affecting load capacity of wall.	Hairline cracks in mortar joints.

Table 4.2 Antiterrorism/Force Protection Design Parameters

<b>Threat Level</b>	<b>Weapon (TNT) (lb*)</b>	<b>Standoff Distance (ft**)</b>	<b>Tool</b>	<b>Blast Pressure using Pentolite (psi***)</b>
High	1000	80	5000 lb truck	≥ 55
Medium	500	80	4000 lb car	31
Low	220	80	4000 lb car	18
Minimum	50	80	4000 lb car	8

\* Convert to Newtons by multiplying by 4.45

\*\* Convert to meters by multiplying by 0.31

\*\*\* Convert to kPa by multiplying by 6.89

## 4.2. TEST MATRIX

A total of eight full-scale walls reflecting different retrofit techniques were included in this study. In these tests, three different types of retrofit techniques were implemented and damage levels to these walls were established as a function of the charge weight and the standoff distance. In this experimental program, the walls were divided into two series. Series I included four walls with nominal dimensions of 88 inches (2.24 m) high by 48 inches (1.22 m) long by 4 inches (100 mm) wide. In this series, the walls were constructed with two-core hollow concrete blocks that had the nominal size of 4 in.  $\times$  8 in.  $\times$  12 in. (102 mm  $\times$  203 mm  $\times$  305 mm). The net area of a block was 18 in<sup>2</sup> (11,610 mm<sup>2</sup>) and the net area compressive strength was 1,520 psi (10,340 kPa) calculated from the average of 4 unit tests. Series II corresponded to the other four walls with nominal dimensions of 88 inches (2.24 m) high by 48 inches (1.22 m) long by 8 inches (203 mm) wide. These four walls in Series II were built with two-core hollow concrete blocks that had the nominal size of 8 in.  $\times$  8 in.  $\times$  16 in. (203 mm  $\times$  203 mm  $\times$  406 mm). The net area of a block was 40 in<sup>2</sup> (25,810 mm<sup>2</sup>) and the net area compressive strength was 1,810 psi (12,480 kPa) calculated from the average of 4 unit tests. The average compressive strength of the mortar used in these series of tests was 1,500 psi (10,340 kPa), according to the ASTM C109 standards. The walls were built by a group of experienced masons using construction techniques representative of good workmanship to not introduce additional variables, such as handwork and different mortar workability that may rise from the construction of the specimens. The specimens were built in two continuous days; half of the wall panel was built during the first day (see Figure 4.1) and the other half was built the following day (see Figure 4.2). Then the

specimens were cured in natural condition for at least thirty days before testing. After that, the FRP rods and/or sheets were applied to the walls as described previously.



Figure 4.1 Construction of the Half Panel

Figure 4.2 Completion of the Whole Wall

A summary of the test matrix is shown in Table 4.3. For Series I, Wall #1 was selected as the un-reinforced control specimen. The remaining three specimens were strengthened with different retrofitting schemes. Thus, Wall #2 was strengthened with 0.25 in. (6.35 mm) GFRP rods at every horizontal joint [i.e. spacing equal to 8 in. (203 mm)]. Wall #3 was strengthened vertically with three 2.5 in. (63.5 mm) wide GFRP strips [i.e. spacing equal to 9.5 in. (241.3 mm)], while Wall #4 was strengthened with both 0.25 in. (6.35 mm) GFRP rods at every horizontal joint and three vertical 2.5 in. (63.5 mm) wide GFRP strips. In this Series, the charges were set up at a standoff distance varying from 6-12 ft (1.83-3.66 m) reflecting different levels of threat.

Series II was divided into two phases depending on the position of the charge from the walls. First phase, called the standoff blast phase, in which the charges were set up at a standoff distance varying from 3-12 ft (0.91-3.66 m) reflecting different levels of threat. In this phase, Wall #5 was selected as the un-reinforced control specimen, while

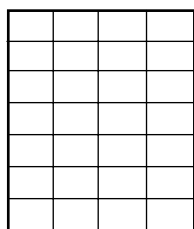
Wall #7 was strengthened with 0.25 in. (6.35 mm) diameter GFRP rods at every horizontal joint [i.e. spacing equal to 8 in. (203 mm)]. In the second phase, called the surface blast phase, the blast charges were installed at mid height of the wall. In this phase, Wall #6 was selected as the un-reinforced control specimen, while Wall #8 was strengthened with both 0.25 in. (6.35 mm) diameter GFRP rods at every horizontal joint and two vertical 4 in. (101.6 mm) wide GFRP strips [i.e. spacing equal to 12 in. (304.8 mm)]. Figure 4.3 shows the three types of retrofitting schemes used in this project.

Table 4.3 Test Wall Matrix Retrofitting Schemes

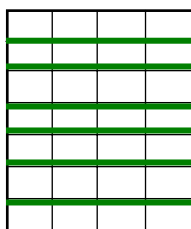
Series Number	Wall Number	Wall Thickness (in)	Symbol
Series I	Wall #1	4	U1
	Wall #2	4	A1
	Wall #3	4	B1
	Wall #4	4	C1
Series II	Wall #5	8	U2
	Wall #6	8	U3
	Wall #7	8	A2
	Wall #8	8	C2

**Legend:** U – Unreinforced                      A – Retrofit A

B – Retrofit B                                      C – Retrofit C

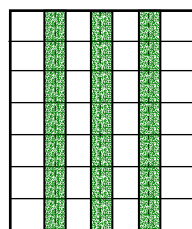


Un-reinforced



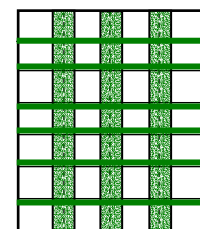
Retrofit A

Horizontal  
FRP Rods



Retrofit B

Vertical  
FRP Sheets



Retrofit C

Vertical FRP Sheets  
& Horizontal FRP Rods

Figure 4.3 Retrofitting Schemes

### 4.3. TEST SETUP

This research program took place at the United States Military Base at Fort Leonard Wood near St. Roberts, Missouri. The tests were conducted on Range 24-Firing Point 4, a certified military explosives range. The eight walls have been constructed on concrete strip footings back-to-back as illustrated in Figure 4.4. The entire testing program consisted of a series of eight of these back-to-back footings as shown in Figure 4.5. The infill walls had boundary members (concrete beam / footing) on the top and bottom of the wall. A structural steel frame was designed to withstand the blast loading and supported the boundary members. The structural steel frame composed of 6 in.  $\times$  6 in.  $\times$  3/8 in. (152.4 mm  $\times$  152.4 mm  $\times$  9.53 mm) tube sections and miscellaneous steel plates and angles as shown in Figure 4.4.

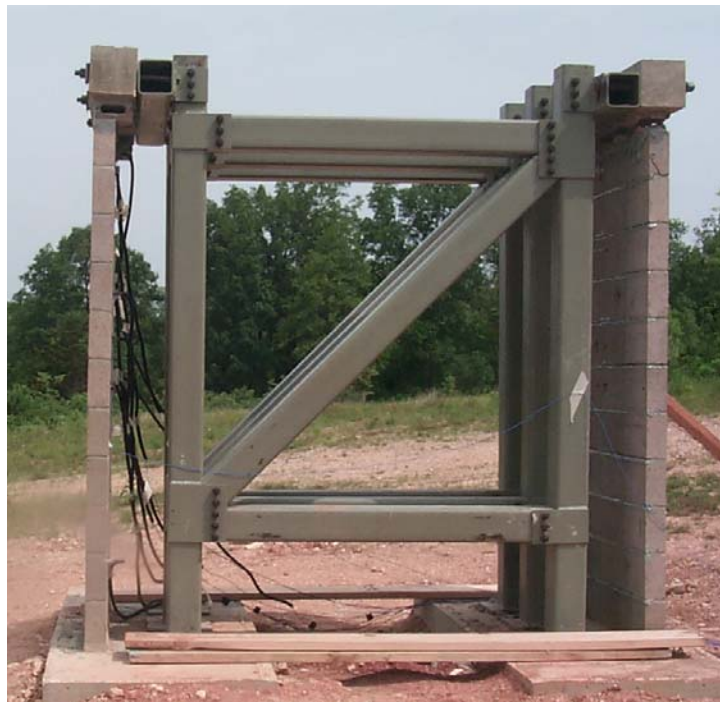


Figure 4.4 Test Setup for Blast Test of URM Walls



Figure 4.5 The Eight Walls Constructed and Prepared for Testing

Conducting these tests required a series of activities. They are listed as follow:

1. Placing the steel frame in position: by means of a crane supplied by the military base. Then it was anchored to the footing.
2. Placing the cap beams: on the top of the back-to-back walls and attached with bolts to the steel frame. One beam was attached to the wall by putty for fast curing while the other kept hanging on the frame. The other wall was supported by braced plywood and a wood shield system to protect it against the blasting that occurred on the other side.
3. Calibration and Installation of instrumentation: It will be fully described in Section 4.4.
4. Blasting and Monitoring: A series of blasts was conducted on the wall reflecting different levels of protection. After each blast, cracks were monitored and marked until failure.
5. Second to fourth activities were repeated again to the mirror wall on the other side of the frame.



6. First to fifth activities were repeated again for the other three sets of back-to-back walls.

#### 4.4. TESTING EQUIPMENT AND INSTRUMENTATION

Two types of data acquisition sensors were used to characterize the pressure wave distribution and displacement of the test walls subjected to the blast loading. These sensors included pressure transducers and accelerometers in conjunction with a data acquisition system of an appropriate sampling rate to capture the blast wave. The pressure transducers were of high frequency ICP pressure sensors 0.218 in. (5.54 mm) diameter probes with measuring range from 2 to 5,000 psi (14 to 34,000 kPa) as shown in Figure 4.6. The accelerometers were of high sensitivity of 100mv/g and of triaxial ICP acceleration sensors with high frequency ranges as shown in Figure 4.8.



Figure 4.6 Pressure Transducer Used in This Study



Figure 4.7 Pressure Transducer Placed at the Front Face of Wall



Figure 4.8 Accelerometer Placed to Back Face of Wall

Six pressure transducers were inserted into the drilled holes on the front face of the wall as shown in Figure 4.7. Six accelerometers were attached to the back face of the wall. Teflon cables of 30 ft (9.14 m) long joined the instrumentation with the data acquisition system (two DAT recorders). The DAT recorders were connected to a portable computer for monitoring and data transfer. Figure 4.9 illustrates the location of the pressure transducers (P) and accelerometers (A) through out the wall area. The instrumentation was calibrated and checked before conducting the test. This phase was only done on the first and second wall in the test series. This phase was necessary to validate the theoretical pressure values obtained from empirical equations with real experimental values. It was also important to calibrate and test our instrumentation before proceeding with the entire test series.

The blast pressure profiles obtained from the pressure transducers will be used in developing a model for predicting the blast peak pressure values at given charge and standoff distance as well as using them with the deflection readings obtained from the accelerometers to analyze the behavior of the URM walls with FRP.

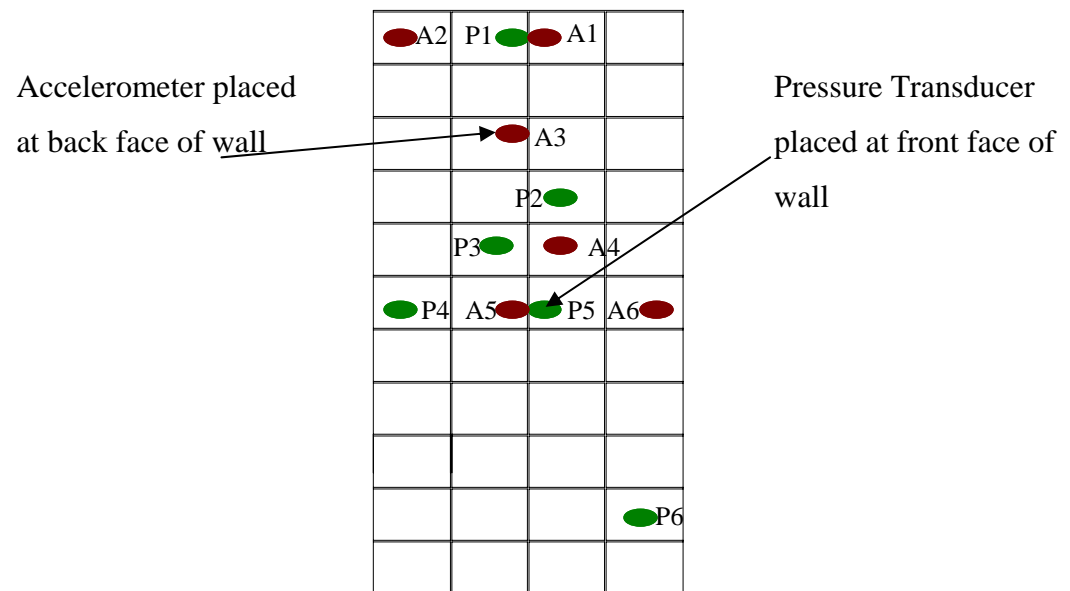


Figure 4.9 Location of Transducers and Accelerometers Throughout the Wall

## 5. PRESSURE ANALYSIS AND MODEL DEVELOPMENT

In this chapter, the blast pressure profiles obtained from the pressure transducers were used in calibrating the instrumentation and in developing a model for predicting the blast peak pressure values at given charge and standoff distance.

### 5.1. PRESSURE CALIBRATION

As mentioned in Section 4.4, small charges of Pentolite dynamite of 0.25 lbs (0.11 kg) at large standoff distances of 16 and 20 ft (4.88 and 6.10 m) were used in this phase (below the minimum threat level standard of the Department of Defense) to validate the theoretical pressure values obtained from the two empirical equations (Model 1 and 2), mentioned previously in Section 2.1.1, with real experimental values obtained from the instrumentation. The values obtained are shown below in Table 5.1.

Table 5.1 Pressure Calibration Stage

<b>Charge Weight and Distance</b>	<b>Experimental Pressure Values (psi*)</b>	<b>Theoretical Pressure Value (Model 1) (psi*)</b>	<b>Theoretical Pressure Value (Model 2) (psi*)</b>
0.25lb@20.05ft	3.24	3.26	0.90
0.25lb@20.1ft	3.27	3.25	0.90
0.25lb@20ft	5.40	3.30	0.91
0.25lb@20.2ft	3.75	3.22	0.88
0.25lb@16ft	5.30	4.52	1.80

\* Convert to kPa by multiplying by 6.89

As observed from Table 5.1, the experimental values obtained from the pressure transducers were exhibited better agreement with Model 1 than from Model 2. Therefore, Model 1 was validated and chosen as a reference for predicted pressure values at different charges and standoff distances. Also, this calibration phase validated the instrumentation setup that was used in this research program.

## 5.2. PRESSURE AND DEFLECTION WAVE RESULTS

Pressure wave profiles were obtained from the instrumentation and validated with the predicted pressure values obtained from Model 1. Figure 5.1 illustrates a typical pressure profile while Figure 5.2 illustrates a wall deflection profile.

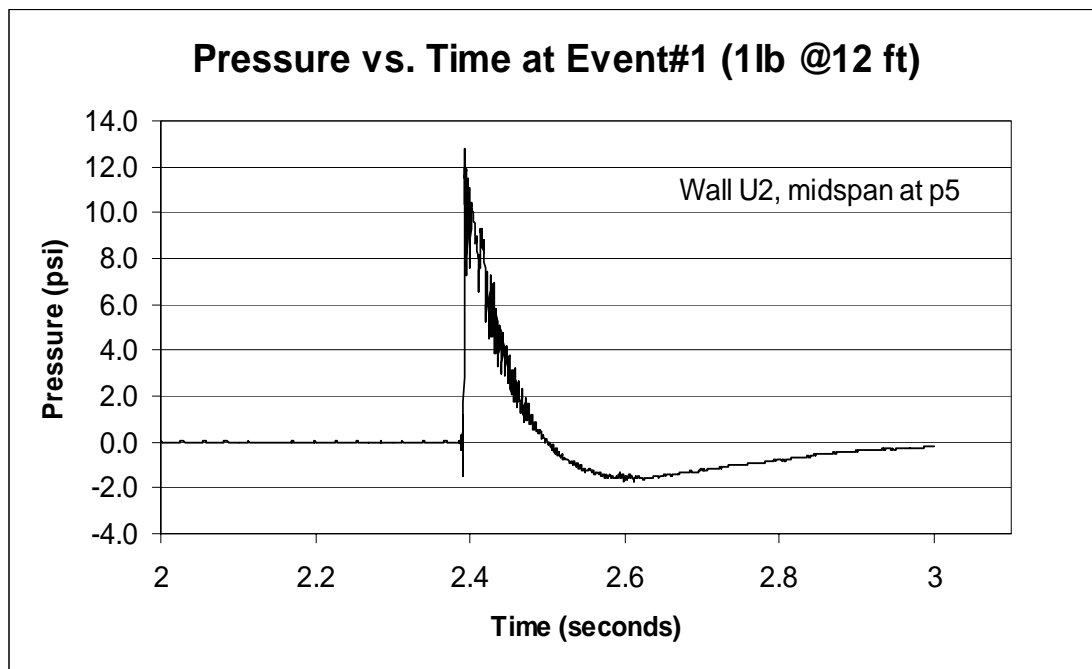


Figure 5.1 Typical Pressure Wave Profile

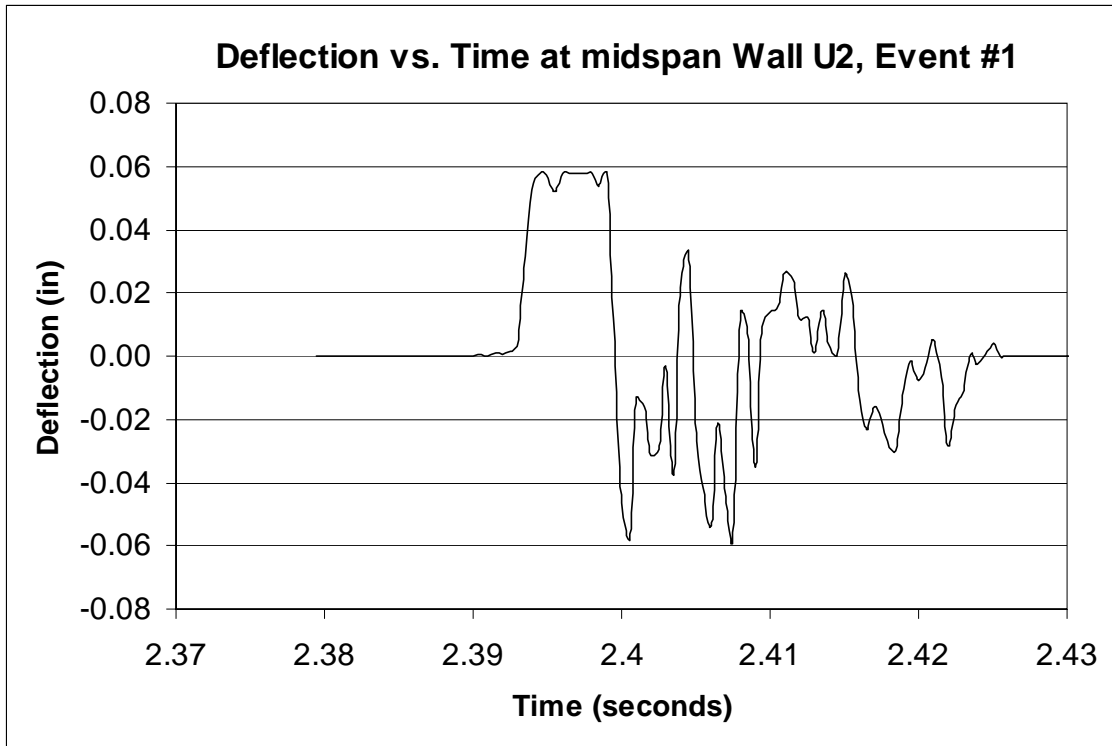


Figure 5.2 Typical Deflection Wave Profile

It is noticed from Figure 5.1 and Figure 5.2 that the maximum deflection of the wall occurs at the same time when the peak pressure hits the wall. For deflection profiles, the accelerometers attached on the back of the wall proved not to be an efficient technique to measure acceleration of the walls. It recorded tremendous amount of noise and was not working properly at higher blast levels. Only two deflection waves were recorded at low blast events for Wall #3 (B1) and Wall #5 (U2) and are shown in Appendix A.1. Table 5.2 shows experimental peak pressures versus predicted peak pressure values from Model 1 at Test Wall #4 (C1). Refer to Appendix A.2 for a complete list of experimental and theoretical pressure values for the rest of the tests. Peak pressure values, time duration of the shock waves and maximum deflections were obtained from the experimental profiles to analyze the walls later in Chapter 6.

Table 5.2 Experimental and Theoretical Peak Pressure Values at Test Wall #4 (C1)

Charge (lb)	Distance (ft)	Peak Pressure (psi *)									
		P2		P3		P4		P5		P6	
		Model 1	Experiment.	Model 1	Experiment.	Model 1	Experiment.	Model 1	Experiment.	Model 1	Experiment.
0.5	12	9.96	9.74	10.03	9.23	9.83	8.4	10.35	11.8	9.52	9.54
1.0	12	15.55	13.78	15.69	13.84	15.31	13.42	16.13	17.3	14.73	13.6
1.5	12	20.88	21.76	21.08	18.1	20.54	20.45	21.54	22.37	19.69	18.54
2.0	12	26.12	24	26.37	26.5	25.67	22.5	26.85	27.5	24.57	22.3
3.0	12	36.36	31.7	36.75	31.8	35.68	33	37.40	35.4	34.03	31.3

\* Convert to kPa by multiplying by 6.89

### 5.3. MODEL DEVELOPMENT FOR PEAK PRESSURE DETERMINATION

Through out this research program, different charges of Pentolite dynamite at varying standoff distances; 3-20 ft (0.91-6.10 m), were used to develop an empirical relationship for pressure distribution based on the measured experimental values obtained. From this data it was observed that there is a linear relationship between charge weight and peak pressure at constant standoff distances as shown in Figure 5.3.

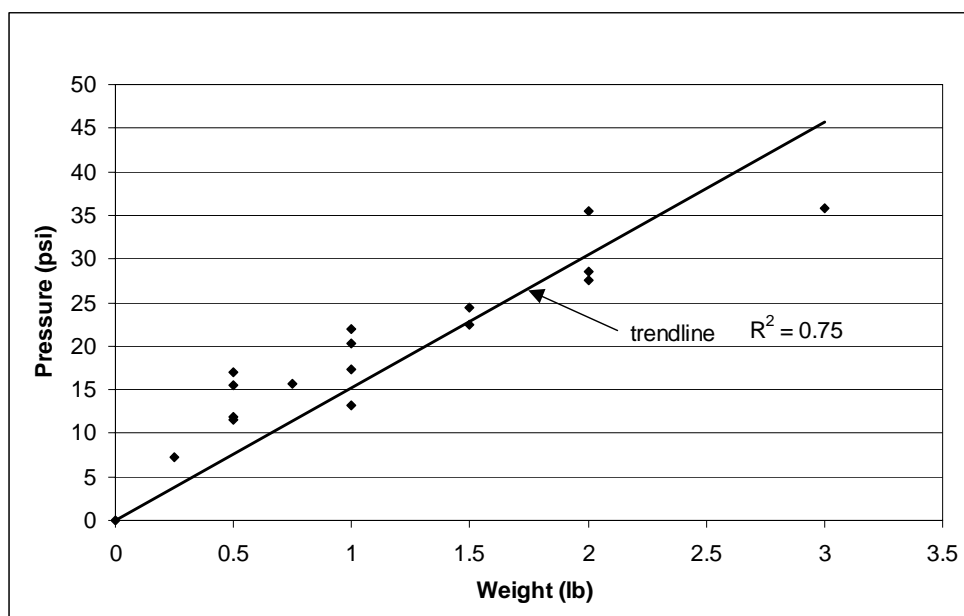


Figure 5.3 Peak Pressure vs. Charge Weight Relationship at 12 ft

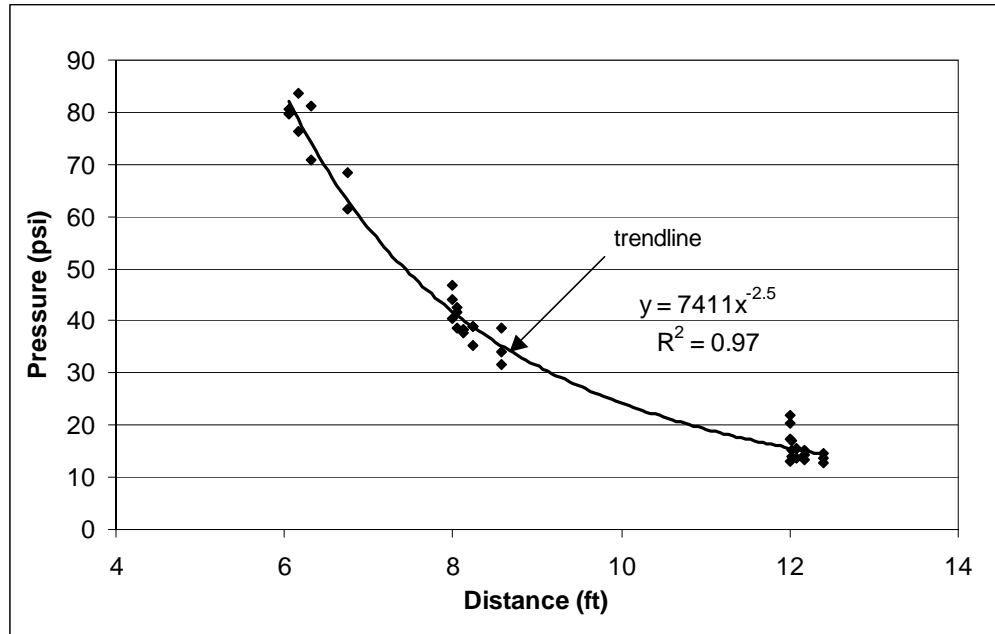


Figure 5.4 Peak Pressure vs. Radial Distance Relationship at 1 lb

It was also observed that there is an interpolated power function relationship between distance and peak pressures at constant charge weights as shown in Figure 5.4. These two relationships led to define a general empirical equation to estimate the peak pressure values at a given weight of charge and standoff distance and this general empirical equation was validated by comparing it with the experimental results and peak pressure values obtained from Model 1. The general empirical equation is:

$$P_{so} = 6670QR^{-2.5} \quad (\text{Equation 5.1})$$

where,

$P_{so}$ : Peak pressure value at given charge weight and standoff distance in psi

$Q$ : Charge weight of Pentolite in pounds

$R$ : Radial standoff distance from the center of the explosive to a particular location on a structure, measured in feet



For design purposes, predicted peak pressure values should be greater than the experimental peak pressure values. Therefore, using a safety factor of 1.2 is preferred when predicting peak pressure values using Equation 5.1. Experimental pressure values below 10 psi (69 kPa) carry some noise and vibration values in their waves, and therefore will be inaccurate and at a higher value than the predicted peak pressure values in that range. See Figure 5.5.

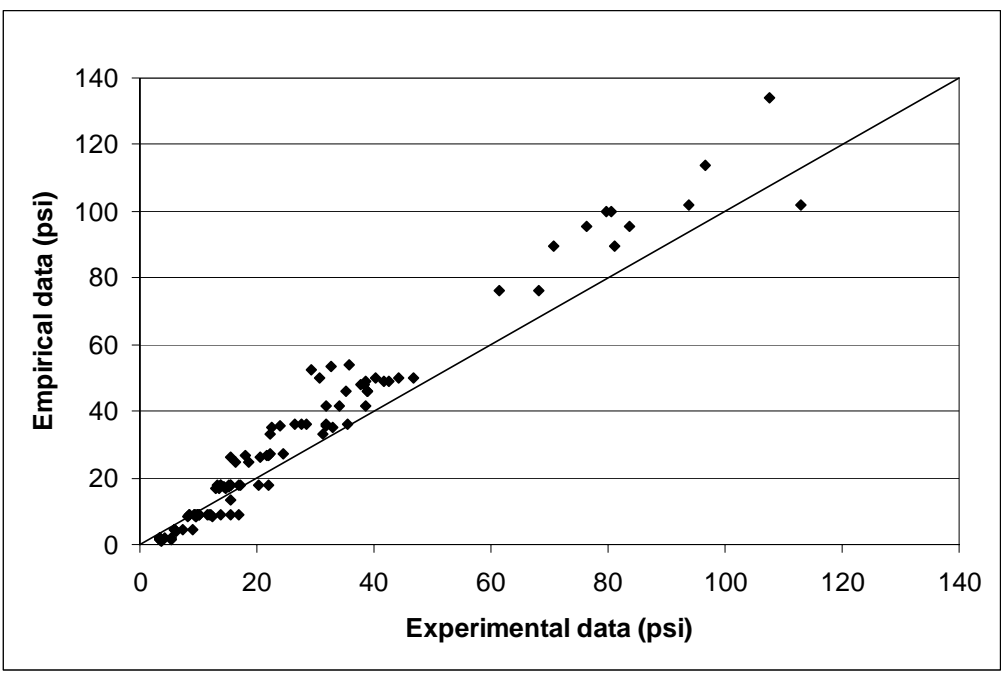


Figure 5.5 Experimental vs. Empirical Model Data

## 6. TEST RESULTS, DISCUSSION AND ANALYTICAL ANALYSIS

### 6.1. TEST RESULTS

Out-of-plane behavior of URM walls is influenced by their boundary conditions, wall to frame connections, height-to-width ratio and their slenderness ratio. In this project, all walls were fixed from the top, simply supported from the bottom and they had a height-to-width ratio of 1.83. Therefore, they were considered to have a one-way out-of-plane flexural behavior.

The walls had no wall-to-frame connections with no restrained sides, which limited their ability to resist rebound forces. Rebound, another important parameter when analyzing or designing structural elements subjected to blast loading can occur after a maximum positive deflection. Blast codes, such as TM 5-1300, require wall to frame connections to assure a proper transfer of these acting forces, or the walls would be limited by their shear capacities at the connections (supports). The rebound forces are usually taken to be equal to the shear resistance of the wall to the blast. Also, the slenderness ratio in Series II walls was 11 while it was 22 for Series I walls. Due to this low slenderness ratio (below than 12.0) in Series II, a higher flexural resistance was expected due to its higher stiffness and stability.

As mentioned previously in Section 4.1 (Experimental Design) that the Interim Department of Defense Antiterrorism/Force Protection Construction Standards requires a minimum threat level with no damage to the structure for design purposes and that the damage occurred to the masonry walls as a result of the blast loading could be measured and correlated to two original parameters: charge weight and standoff distance. This correlation would indicate key relationships and provide insight for conducting risk

assessment and determining acceptable levels of protection for walls under such blast loadings. Therefore, this section provides full descriptions of the behavior of the walls and the correlated damage and threat levels are described below.

### 6.1.1. Results of Series I - 4 in. CMU Walls:

#### Wall U1

This wall was tested as a control unit for Series I to determine the maximum blasting capacity of a 4 in. (100 mm) URM wall. This wall was subjected to six events of blast loads reflecting different hazard levels until failure. Table 6.1 lists the blast events applied to wall U1 with the corresponding peak pressure values (mid-height) and correlated damage and threat levels. Refer to Appendix A.2 to view detailed pressure data at other positions of the wall for different events.

Table 6.1 Blast Events vs. Damage and Threat Levels Correlations of Wall U1

Event #	Charge (lb*)	Standoff Distance (ft**)	Peak Pressure (psi***)	Damage Level	Threat Level
1	0.50	16	6.5	No Damage	Minimum
2	0.25	12	7.0	No Damage	Minimum
3	0.50	12	10.5	No Damage	Low
4	1.0	8	41.0	No Damage	High
5	1.5	6	136.0	Light Damage	High
6	2.0	6	182.0	Failure (Flexural)	High

\* Convert to Newtons by multiplying by 4.45

\*\* Convert to meters by multiplying by 0.31

\*\*\* Convert to kPa by multiplying by 6.89

It was observed in event #1 that vertical hairline cracks were developed along the full mortar bed joints at the front face of the wall due to lack of vertical constraints along the sides of the wall. Due to event #2 and 3, vertical hairline cracks further developed along the full mortar bed joints at the back face of the wall. Horizontal hairline cracks developed in event #4 along most of the bed joints at the back face of the wall. Furthermore, a horizontal crack along the base bed of the wall developed. Due to event #5, more horizontal cracks on the backside of the wall were observed as well as cracks along the majority of the bed joints on the front face of the wall. Previous cracks widths increased as shown in Figure 6.1 due to subsequent blast events. Brittle out of plane failure occurred due to event #6, where the wall collapsed into debris towards the backside direction of the wall as shown in Figure 6.2.

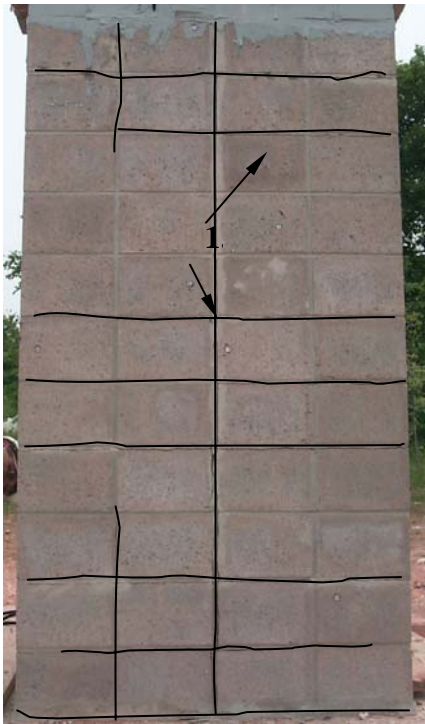


Figure 6.1 Wall U1 after Event #5



Figure 6.2 Failure of Wall U1 after Event #6

### Wall A1

This wall was retrofitted on the backside with 0.25 in. (6.35 mm) diameter GFRP rods at every horizontal joint [i.e. spacing equal to 8 in. (203 mm)]. This wall was subjected to six events of blast loads reflecting different hazard levels. Failure was not achieved here due to site limitations, but still a comparison can be made with the behavior of wall U1 at different blast events. Table 6.2 lists the blast events applied to wall A1 with the corresponding peak pressure values (mid-height) and correlated damage and threat levels. Refer to Appendix A.2 to view detailed pressure data at other positions of the wall for different events.

Table 6.2 Blast Events vs. Damage and Threat Levels Correlations of Wall A1

Event #	Charge (lb*)	Standoff Distance (ft**)	Peak Pressure (psi***)	Damage Level	Threat Level
1	0.5	12	10.5	No Damage	Low
2	0.75	12	13.5	No Damage	Low
3	1.0	12	16.0	No Damage	Low
4	1.5	12	21.5	No Damage	Medium
5	2.0	12	27.0	Light Damage	Medium
6	3.0	12	37.0	Light Damage	High

\* Convert to Newtons by multiplying by 4.45

\*\* Convert to meters by multiplying by 0.31

\*\*\* Convert to kPa by multiplying by 6.89

There were no cracks observed visually after event #1 and event #2. Due to event #3, vertical hairline cracks developed along the full mortar bed joints at the front face of the wall due to lack of vertical constraints along the sides of the wall. Due to event #4, discontinuous vertical hairline cracks developed along the full mortar bed joints at the back face of the wall. Horizontal hairline cracks initiated due to event #5 along most of the mortar bed joints on the front face and along the epoxy joints on the back face of the wall. Figure 6.3 shows a horizontal crack along the mid-height epoxy joint on the back face of the wall taken after event #5. In addition, a horizontal crack along the base bed of the wall and shear hairline cracks developed at the top support of the wall. Due to event #6, cracks became wider in both horizontal and vertical directions on the front and back face of the wall. Shear cracks also increased in size as shown in Figure 6.4 while Figure 6.5 shows the cracks developed at the front face of the wall after Event #6.

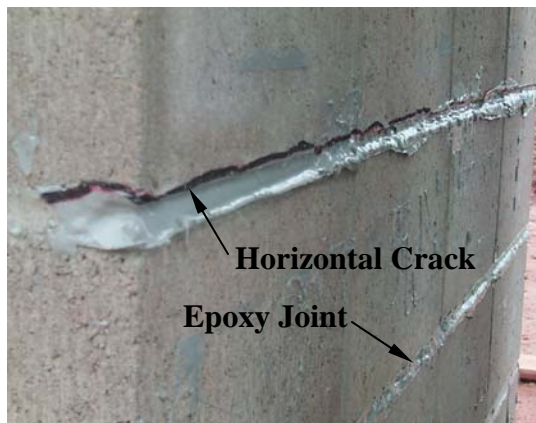


Figure 6.3 Horizontal Crack in Epoxy Joint in Wall A1 after Event #5

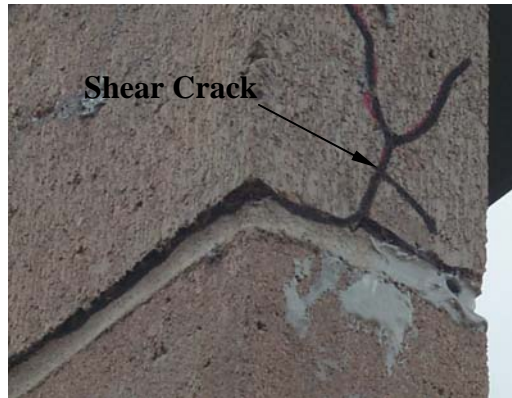


Figure 6.4 Shear Crack at Top Support of Wall A1 at Event #6

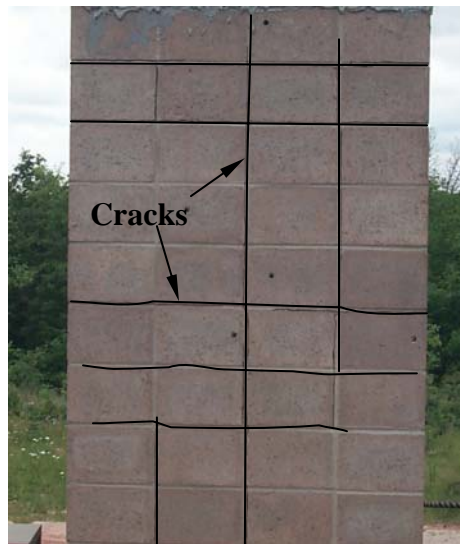


Figure 6.5 Cracks at Front Face of Wall A1 after Event #6

### Wall B1

This wall was retrofitted on the backside vertically with three 2.5 in. (63.5 mm) wide GFRP strips [i.e. spacing equal to 9.5 in. (241.3 mm)]. This wall was subjected to six events of blast loads reflecting different hazard levels till failure. Table 6.3 lists the blast events applied to wall B1 with the corresponding peak pressure values (mid-height) and correlated damage and threat levels. Refer to Appendix A.2 to view detailed pressure data at other positions of the wall for different events.

Table 6.3 Blast Events vs. Damage and Threat Levels Correlations of Wall B1

<b>Event #</b>	<b>Charge (lb*)</b>	<b>Standoff Distance (ft**)</b>	<b>Peak Pressure (psi***)</b>	<b>Damage Level</b>	<b>Threat Level</b>
1	0.5	16	6.5	No Damage	Minimum
2	0.5	12	10.5	No Damage	Low
3	1.0	12	16.0	No Damage	Low
4	1.5	12	21.5	No Damage	Medium
5	2.0	12	27.0	Light Damage	Medium
6	3.0	12	37.0	Heavy Damage (Shear Damage)	High
7	2.0	6	182.0	Failure (Flexural)	High

\* Convert to Newtons by multiplying by 4.45

\*\* Convert to meters by multiplying by 0.31

\*\*\* Convert to kPa by multiplying by 6.89

There were no cracks observed after events #1 and 2. Due to event #3, vertical hairline cracks were developed along the full mortar bed joints at the front face of the wall due to lack of vertical constraints along the sides of the wall. Due to event #4, more vertical hairline cracks were observed along the full mortar bed joints at the front face of the wall. Horizontal cracks began to develop after event #5 along most of the bed joints at the back face of the wall. Furthermore, shear hairline cracks developed at the top support of the wall. In addition to that, a horizontal crack along the base bed of the wall and the vertical cracks increased in width. Due to event #6, shear cracks increased in size, reducing the top support of the wall shear capacity to resist rebound forces as shown in Figure 6.6 and the vertical and horizontal cracks widened up on the front and back face of



the wall. No significant damage was observed on the tension face due to the initial shock waves. Out of plane failure occurred due to event #7 (see Figure 6.7), where the wall collapsed into two contact units towards the front side of the wall's position due to rebound pressure as shown in Figures 6.7 (a) through (c).

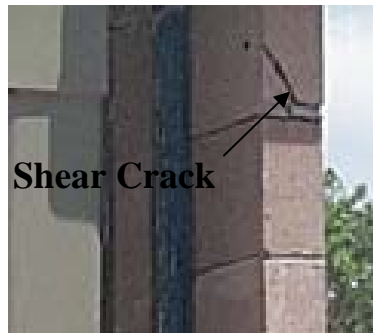


Figure 6.6 Shear Crack at Top Support of Wall B1 after Event #6



(a) Wall B1 during the Explosion



(b) Out-of-Plane Failure



(c) Wall B1 Collapsed

Figure 6.7 Collapse Failure of Wall B1 after Event #7

### Wall C1

This wall was strengthened on the backside with both 0.25 in. (6.35 mm) diameter GFRP rods at every horizontal joint and three vertical 2.5 in. (63.5 mm) wide GFRP strips. This wall was subjected to seven events of blast loads reflecting different hazard levels until failure. Table 6.4 lists the blast events applied to wall C1 with the corresponding peak pressure values (mid-height) and correlated damage and threat levels. Refer to Appendix A.2 to view detailed pressure data at other positions of the wall for different events.

Table 6.4 Blast Events vs. Damage and Threat Levels Correlations of Wall C1

Event #	Charge (lb*)	Standoff Distance (ft**)	Peak Pressure (psi***)	Damage Level	Threat Level
1	0.5	12	10.5	No Damage	Low
2	1.0	12	16.0	No Damage	Low
3	1.5	12	21.5	No Damage	Medium
4	2.0	12	27.0	Light Damage	Medium
5	3.0	12	37.0	Light Damage	High
6	2.0	6	182.0	Heavy Damage (Shear Damage)	High
7	3.0	6	274.0	Failure (Flexural)	High

\* Convert to Newtons by multiplying by 4.45

\*\* Convert to meters by multiplying by 0.31

\*\*\* Convert to kPa by multiplying by 6.89

There were no cracks observed after event #1 and event #2. Due to event #3, discontinuous vertical hairline cracks were developed along the full mortar bed joints at the front face of the wall due to lack of vertical constraints along the sides of the wall. After event #4, more vertical hairline cracks were observed along the full mortar bed joints at the front and back face of the wall. Horizontal cracks also developed along the top and base bed joints of the wall on the front face. More horizontal and vertical cracks were observed after event #5 along most of the mortar bed joints on the front face of the wall. Also there were shear hairline cracks that developed at the top support of the wall as shown in Figure 6.8. Due to event #6, more horizontal and vertical cracks were detected and previous cracks increased in width on the front face of the wall as shown in Figure 6.9. Also, shear cracks increased in size weakening the top support of the wall to resist rebound forces. Progressive out of plane failure occurred after event #7, where the wall collapsed into two contact units towards the front side of the wall's position due to rebound pressure as shown in Figure 6.10.



Figure 6.8 Shear Crack at Top Support of Wall C1 after Event #5



Figure 6.9 Front Face of C1 after Event #6    Figure 6.10 Collapse of C1 after Event #7

**6.1.2. Results of Series II - 8 in. CMU Walls:** This series was divided into two phases depending on the position of the charge from the walls. First phase was called the standoff blast phase, while the second phase was called the surface blast phase.

#### **6.1.2.1 Standoff blast phase:**

##### **Wall U2**

This wall was tested as a control unit to determine the maximum blasting capacity of an URM 8 in. (203 mm) thick wall subjected to distant blast loads. This wall was subjected to seven events of blast loads reflecting different hazard levels until failure. Table 6.5 lists the blast events applied to wall U2 with the corresponding peak pressure values (mid-height) and correlated damage and threat levels. Refer to Appendix A.2 to view detailed pressure data at other positions of the wall for different events.

It was observed after event #1 that vertical hairline cracks were developed along the full mortar bed joints at the front face of the wall due to lack of vertical constraints

along the sides of the wall. Due to event #2, vertical hairline cracks were also developed along the mortar bed joints at the back face of the wall. Horizontal hairline cracks began to develop also along the mid-height bed joint at the back face of the wall and along the base bed of the wall.

Table 6.5 Blast Events vs. Damage and Threat Levels Correlations of Wall U2

<b>Event #</b>	<b>Charge (lb*)</b>	<b>Standoff Distance (ft**)</b>	<b>Peak Pressure (psi***)</b>	<b>Damage Level</b>	<b>Threat Level</b>
1	1.0	12	16	No Damage	Low
2	1.0	8	41	No Damage	High
3	1.0	6	91	No Damage	High
4	1.5	6	136	No Damage	High
5	2.0	6	182	Light Damage	High
6	3.0	6	274	Light Damage	High
7	7.5	6	683	Heavy Damage	High

\* Convert to Newtons by multiplying by 4.45

\*\* Convert to meters by multiplying by 0.31

\*\*\* Convert to kPa by multiplying by 6.89

Due to event #3, discontinuous horizontal cracks were also observed along most of the bed joints on the front and back face of the wall and the previous cracks increased in size. The cracks in both the horizontal and vertical directions got wider after event #4. Due to event #5, the vertical cracks got deeper especially along the first bed joint extending from mid-height till the ground base of the wall weakening the vertical bed

joints as shown in Figure 6.11. Failure without collapse occurred after event #6, where the vertical crack in the first joint split 1/3 of the wall as shown in Figures 6.12 and 6.13. Due to event #7, progressive failure and damage occurred to the splitting portion of the wall and some debris was scattered as shown in Figure 6.14.

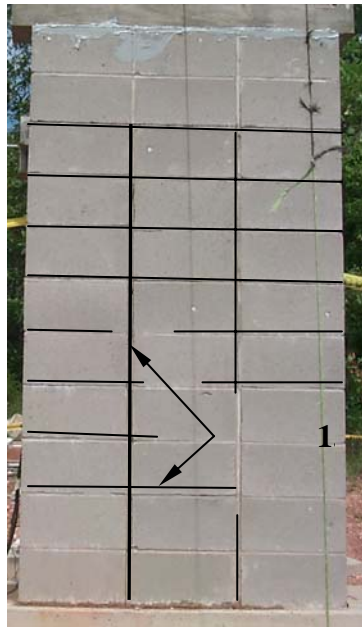


Figure 6.11 Cracks of U2 after Event #5

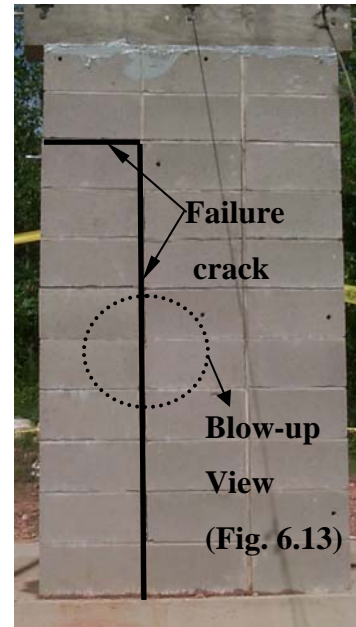


Figure 6.12 Failure of U2 after Event #6

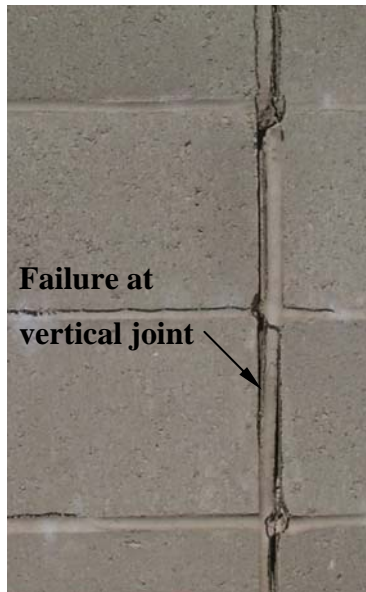


Figure 6.13 Blow-up View after Event #6

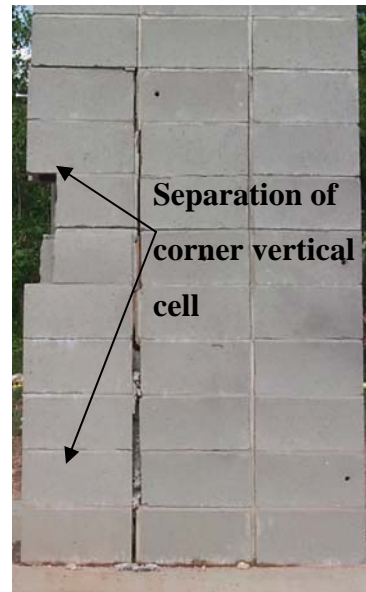


Figure 6.14 Wall U2 after Event #7

## Wall A2

This wall was strengthened with 0.25 in. (6.35 mm) diameter GFRP rods at every horizontal joint [i.e. spacing equal to 8 in. (203 mm)]. This wall was subjected to seven events of blast loads reflecting different hazard levels until failure. Table 6.6 lists the blast events applied to wall A2 with the corresponding peak pressure values (mid-height) and correlated damage and threat levels. Refer to Appendix A.2 to view detailed pressure data at other positions of the wall for different events.

Table 6.6 Blast Events vs. Damage and Threat Levels Correlations of Wall A2

Event #	Charge (lb)	Standoff Distance (ft)	Peak Pressure (psi*)	Damage Level	Threat Level
1	1	12	16	No Damage	Low
2	1	8	41	No Damage	High
3	1	6	91	No Damage	High
4	2	6	182	No Damage	High
5	3	6	274	Light Damage	High
6	5	6	460	Heavy Damage (Shear failure)	High
7	3	3	1940	Failure	High

\* Convert to Newtons by multiplying by 4.45

\*\* Convert to meters by multiplying by 0.31

\*\*\* Convert to kPa by multiplying by 6.89

It was observed after event #1 that vertical hairline cracks developed along the full mortar bed joints at the front face of the wall due to lack of vertical constraints along

the sides of the wall. Due to event #2, vertical hairline cracks also developed along the mortar bed joints at the back face of the wall. A horizontal hairline crack began to develop after event #3 along the mid-height epoxy based bed joint at the back face of the wall. Also there was a horizontal crack along the base bed of the wall and some discontinuous vertical cracks on the front face of the wall. Due to event #4, a horizontal crack was also observed along the top bed joint on the front and back face of the wall. The cracks in both the horizontal and vertical directions increased in size after event #5. Due to event #6, shear failure along with a significant horizontal crack in the top bed joint occurred at the top support of the wall as shown in Figure 6.15 and 6.16. Also, there was a wide horizontal crack at mid-height of the wall and some blocks on the corner were broken as shown in Figure 6.17. The broken parts were hold by the FRP rods preventing them to fall on the backside of the wall. Wide vertical cracks also occurred on the front and backside of the wall. Progressive failure with collapse into crumbles occurred in event #7, where the debris was towards the front side of the wall's position as shown in Figure 6.18.



Figure 6.15 Shear Failure after Event #6

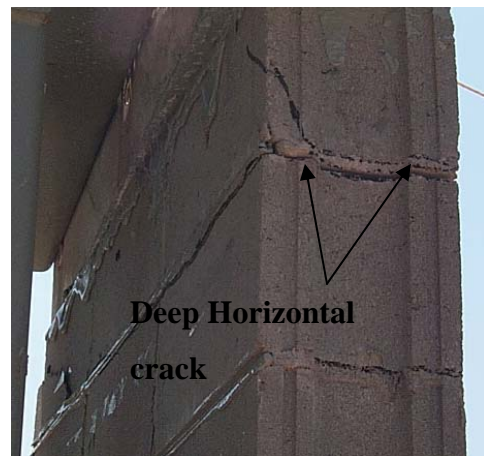


Figure 6.16 Horizontal Crack after Event #6





Figure 6.17 Wall A2 after Event #6



Figure 6.18 Collapse of A2 after Event #7

### 6.1.2.2 Surface blast phase

#### Wall U3

This wall was tested as a control unit to determine the behavior of an URM 8 in. (203 mm) thick wall subjected to blast loads that are in contact to its surface at mid-height. This wall was subjected to two events of blasting. One pound (4.48 N) of Pentolite was discharged on the first event and a hole was punched at mid-height through the masonry wall where there was more damage on the backside of the wall as seen in Figures 6.19 and 6.20. It was noticed that the debris was thrown to a distance almost 8 ft (2.44 m) from the backside of the wall. There were also, vertical and horizontal cracks in the bed joints on the front and backside of the wall. Wall U3 experienced a level of heavy damage and a high threat at event #1. Due to event #2, 2 lb (8.9 N) of Pentolite were discharged and a progressive failure of most of the wall occurred. Most of the debris was scattered away to a distance of 10 ft (3.05 m). Wall U3 experienced a level of failure due to event #2.



Figure 6.19 Front Side of U3 after Event #1    Figure 6.20 Backside of U3 after Event #1

### Wall C2

This wall was strengthened with both 0.25 in. (6.35 mm) diameter GFRP rods at every horizontal joint and two vertical 4 in. (100 mm) wide GFRP strips [i.e. spacing equal to 12 in. (304.8 mm)]. This wall was subjected to three events of blasting. One pound (4.48 N) of Pentolite was discharged on the first event and a hole was punched at mid-height through out the masonry wall where there was more damage on the backside of the wall as seen in Figures 6.21 and 6.22. It was noticed that the debris fell right behind the wall. There were also, vertical and horizontal cracks in the bed joints on the front and backside of the wall. Due to event #2, 2 lb (8.9 N) of Pentolite was discharged with a progressive failure of the middle blocks of the wall as shown in Figure 6.23. Most of the debris was right behind the wall. Wall C2 experienced heavy damage and high threat levels after events #1 and 2. In event #3, 5 lb (22.24 N) of Pentolite was discharged with a complete collapse of the wall as shown in Figure 6.24. Most of the debris was at the same location of the wall and right behind it. It was also noticed that during these three events the FRP rods and sheets did not rupture or tear from these surface blasts.



Figure 6.21 Front Side of Wall C2 after Event #1



Figure 6.22 Side View of C2 after Event #1    Figure 6.23 Side View of C2 after Event #2



Figure 6.24 Total Collapse of Wall C2 after Event #3

## 6.2. TEST DISCUSSION

Masonry walls subjected to blast loads can fail in at least three failure modes; tensile failure in zones of high flexure, compressive failure in zones of high flexure, and shear failure near the supports. The walls resist out-of-plane load in the flexural response mode, which creates areas of high moment in the wall. The moment causes tensile strain on the backside face of the wall and compressive strain on the front face facing the blast. Either these strains can exceed the tensile or compressive failure strain of the reinforced wall and cause flexural failure. Flexural response also causes shear stresses near the supports. Additional shear stresses are caused due to rebound forces and negative blast pressures. These stresses can cause shear failure if they exceed the shear strength of the masonry, since there are no wall to frame connections. Shear strength of masonry walls is typically calculated based on the Building Code Requirements for Masonry Structures 1999 and the Uniform Building Code 1994 as shown in Equation 6.1. Only the webs of

the blocks provide the shear strength since all of the walls in this research program are un-grouted walls.

$$V_n = 1.5\sqrt{f'_m} \text{ , where} \quad \text{(Equation 6.1)}$$

$V_n$  : masonry shear strength over affective shear area (psi)

$f'_m$  : masonry unit prism compressive strength (psi)

**6.2.1. Un-reinforced Masonry Walls Behavior:** Un-reinforced concrete masonry walls have a high compressive resistance but have a low tensile resistance. Also, the low rebound forces applied from the plastic behavior of URM walls with the low negative blast pressures are below the shear capacity of the un-reinforced concrete masonry walls. Therefore, the blast capacity of un-reinforced concrete masonry walls will typically be limited by their tensile capacity. Then the URM walls only fail out of plane in a tensile failure mode in zones of high flexure.

This behavior was observed in wall U1. The wall experienced vertical and horizontal cracks through out the blast events until it suffered a brittle tensile failure at its horizontal mid-height mortar joint at blast peak pressure of 182 psi (1254 kPa) that resulted in collapsing of the wall (See Figure 6.2).

Wall U2 had a higher out-of-plane flexural resistance than wall U1 due to its lower slenderness ratio. There were horizontal cracks at high blast levels due to the partial out-of-plane behavior but did not affect the flexural capacity of wall U2. The lack of vertical constraints to the wall with the blast pressure wrapping on its sides and its low slenderness ratio, resulted in a different behavior than the behavior of wall U1. The vertical cracks developed at the lower blast levels controlled the behavior of this wall.

The corner vertical cells were rotating due to the pressure wrap. Therefore, the vertical mortar joints were always facing tensile strains on the face of the wall and compression at the backside. This behavior resulted in splitting one corner vertical cell of the wall from the rest of it due to tensile failure of the vertical joint at the face of the wall (See Figure 6.14).

**6.2.2. FRP Retrofitted Masonry Walls Behavior:** In walls retrofitted with FRP, the FRP resist practically the tensile stress caused by the flexural response. The masonry cracked at the bed joints at very low stress level and did not resist any tensile stress beyond cracking stress. However the concrete masonry resists most of the compressive stress. Rebound forces resulted from the elastic behavior of the applied FRP to these walls could be higher than the shear capacity of the masonry walls. There were no wall-to-frame connections for the retrofitted walls in this research program to transfer the rebound forces that resulted. Therefore, the blast capacity of these reinforced concrete masonry walls would typically be limited by their shear capacity expressed in Equation 6.1. As implied in Equation 6.1, the FRP reinforcement does not contribute to the shear strength of the masonry walls. Although the FRP reinforcement may provide some amount of confinement that increases the shear strength of the masonry walls, there is no available data that confirms this statement. Therefore, URM walls retrofitted with FRP are more likely to fail or be heavily damaged in zones of high shear stresses and would not survive additional blast loads without collapsing in an out of plane manner.

**6.2.2.1 FRP retrofitted masonry walls in series I:** Wall A1, retrofitted with 0.25 in. (6.35 mm) diameter GFRP rods horizontally at every bed joint, had hairline shear cracks along with horizontal and vertical cracks at blast peak pressures of 27 and 37 psi

(186 and 248 kPa). These blast pressures caused light damage levels due to the presence of hairline shear cracks.

Wall B1, retrofitted with three GFRP strips 2.5 in. (63.5 mm) wide, had a light damage level with hairline shear cracks at the same level of blast peak pressure of 27 psi (186 kPa) but it experienced shear damage at the blast peak pressure of 37 psi (248 kPa) that caused high damage to the wall. The shear damage resulted from high shear stresses and rebound forces caused from the elastic behavior of the GFRP sheets at this blast level that weakened the wall's top support to resist higher blast loads. It failed in an out-of-plane flexural manner towards the front side of the wall due to the rebound forces caused from the elastic rebound behavior of the GFRP sheets at a blast pressure of 182 psi (1254 kPa).

On the other hand, wall C1, reinforced with both 0.25 in. (6.35 mm) diameter GRP rods at every horizontal bed joint and three GFRP strips, had light damage levels with hairline shear cracks at both blast peak pressures of 27 and 37 psi (186 and 248 kPa). It experienced shear damage at blast peak pressure of 182 psi (1254 kPa) that caused high damage to the wall. The shear damage resulted from high shear stresses and rebound forces caused from the elastic behavior of the GFRP sheets at this blast level. This behavior weakened the wall's top support to resist higher blast loads. It collapsed in an out-of-plane flexural manner towards the front side of the wall due to the rebound forces caused from the elastic rebound behavior of the GFRP sheets at a blast peak pressure of 274 psi (1889 kPa).

The retrofitting schemes changed the behaviors of walls B1 and C1 with the unreinforced masonry control unit wall U1. Wall U1 had no damage at blast pressures of 27

and 37 psi (186 and 248 kPa) and had a brittle sudden flexural failure at blast pressure of 182 psi (1254 kPa). Wall C1 had an increase in its blast capacity than the un-reinforced wall U1, while wall B1 blast capacity was reduced because of shear limitations. It was expected that wall A1 would have a blast capacity between the blast capacities of U1 and C1.

From the results and observations obtained from Series I, it was concluded that 4 in. (100 mm) un-reinforced concrete masonry walls with same boundary conditions, slenderness and height to width ratios as in this research program will meet the DOD requirements to resist a minimum threat level with no damage.

It was also concluded that increasing the out-of-plane flexural capacity of 4 in. (100 mm) URM walls to resist higher threat levels with lower damage levels meeting the DOD requirements has to be associated with proper wall to frame connections with increasing shear capacity by grouting the wall or reducing span length to resist shear stress and transfer the rebound forces resulted from the retrofit or else the retrofitted wall blast capacity will reduce, as the reinforced wall's shear capacity controls.

The horizontal GFRP bars reinforcement provided some amount of confinement, stiffness and crack control of the reinforced masonry walls to resist the blast and rebound loads. This has been illustrated with the behavior of wall A1 that experienced light damage with hairline shear cracks at blast pressure of 37 psi (248 kPa) while wall B1 experienced heavy shear damage at the same amount of pressure. Also, the horizontal bars helped wall C1 in resisting the blast pressure of 182 psi (1254 kPa) and experienced heavy shear damage without collapse while wall B1 collapsed at that same blast level. It



may be concluded that the hybrid retrofitting system increased the overall blast capacity of wall C1.

Shear damage in retrofitted walls was an indication of a brittle behavior and an indication for not surviving additional blast loads and that the retrofitted walls' collapse towards the outside direction in contact debris would help in reducing the hazard of causing harm and injury to building occupants.

**6.2.2.2 FRP retrofitted masonry walls in series II:** As mentioned before, this series was divided into two phases depending on the position of the charge from the walls. Each phase is discussed individually.

**6.2.2.2.1 Standoff blast phase:** Wall A2 was retrofitted with 0.25 in. (6.35 mm) diameter GFRP rods horizontally at every bed joint. The presence of horizontal bars acting as vertical constraints to the wall prevented the corner vertical cells from rotating and controlled the vertical cracks with the blast pressure wrapping on its sides. This resulted in an out-of-plane flexural behavior different than the behavior of wall U2.

Hairline shear cracks along with horizontal and vertical cracks were observed at blast peak pressure of 274 psi. This blast pressure caused a light damage level due to the presence of hairline shear cracks. It experienced shear damage at blast peak pressure of 460 psi that caused high damage to the wall. The shear damage resulted from high shear stresses and rebound forces at this blast level weakened the wall's top support to resist higher blast loads. It failed in an out-of-plane flexural manner towards the front side of the wall due to the rebound forces caused from the elastic behavior of the GFRP rods at a blast peak pressure of 1940 psi (13.4 MPa).

Comparing behavior of wall A2 with the un-reinforced masonry control unit wall U2, the horizontal reinforcement enhanced the flexural capacity of wall A2 by limiting the rotation and splitting of the vertical cells of the wall in the transverse direction (See Figure 6.17). Therefore the overall blast capacity of wall A2 increased than the un-reinforced wall.

From the results and observations obtained from Series II, it was concluded that 8 in (203 mm) un-reinforced concrete masonry walls with same slenderness and height to width ratios as in this research program will meet the DOD requirements to resist a minimum threat level with no damage.

It was also concluded that increasing the out-of-plane flexural capacity of 8 in. (203 mm) URM walls to resist higher threat levels with lower damage levels meeting the DOD requirements has to be associated with proper wall to frame connections with increasing shear capacity by grouting the wall or reducing span length to resist shear stresses and transfer the rebound forces resulted from the retrofit or else the retrofitted wall blast capacity will reduce, as the reinforced wall's shear capacity controls (See Figure 6.15). The failure of the wall A2 was towards the front side would help in reducing the hazard of harm and injury to building occupants resulting from wall debris blasted at high velocity, while wall U2 tended to fail at the back side direction increasing the threat of harm and injury to occupants within the space (See Figure 6.18).

**6.2.2.2.2 Surface blast phase:** In this phase, wall C2, strengthened with both 0.25 in. (6.35 mm) diameter GRP rods at every horizontal bed joint and three GFRP strips, had a collapse failure at a surface mid-height blast of 5 pounds (22.24 N) of Pentolite, while the un-reinforced wall U3 collapsed at a surface mid-height blast of 2 pounds (8.9 N) of

Pentolite. Therefore, the FRP strengthening increased the blast capacity of wall C2 (see Figure 6.22) with debris right behind the walls position that would help in reducing the hazard of injury and death to building occupants resulting from wall debris blasted at high velocity as in the case of wall U3. Also, the FRP bars and sheets did not rupture or tear from the high impact surface blast loads, so increasing the FRP reinforcement could improve the surface blast capacities and threat levels of these walls.

### 6.3. ANALYTICAL STUDY

The basic analytical model used in most blast analysis and design applications is the single degree of freedom (SDOF) system. The use of the SDOF approach to predict the dynamic response of simple structural elements, such as walls, is well documented in a number of sources including ASCE-Design of Blast Resistant Buildings (1997) and the Departments of the Army, Navy and Air Force-TM5-1300 (1990) Code. The dynamic equilibrium of damped, linear elastic, SDOF system is expressed mathematically in Equation 6.2.

$$Ma + CV + Ky = F(t), \text{ where} \quad (\text{Equation 6.2})$$

$M =$  mass

$a =$  acceleration

$C =$  viscous damping force

$V =$  velocity

$K =$  stiffness

$y =$  displacement

$F(t) =$  applied force as a function of time

. Due to the short time in which the structure reaches its maximum response, damping effects have little effect on peak displacements. Therefore, Damping is usually conservatively ignored in blast resistant design. As a result, the dynamic equilibrium equation for un-damped, elastic system is expressed in Equation 6.3

$$Ma + Ky = F(t) \quad (\text{Equation 6.3})$$

In blast analysis, the resistance is usually specified as a nonlinear function to simulate elastic, perfectly plastic behavior of the structure. The ultimate resistance,  $R_u$ , is reached upon formation of a collapse mechanism in the member. When the resistance is nonlinear, the dynamic equilibrium equation is expressed in Equation 6.4

$$Ma + R = F_t, \text{ where} \quad (\text{Equation 6.4})$$

$$R = \text{lesser of } Ky \text{ or } R_u$$

The procedure for obtaining the equivalent SDOF approximation for a structural component is based on its deformed shape under the applied loading and the strain energy equivalence between the actual structure and the SDOF approximation. In addition to strain energy equivalence, the motion of the SDOF system is equivalent to a selected control point on an actual structure. The control point is usually selected at a point of maximum response such as a plastic hinge location within the span. However, the spring force is not equal to the support reactions of the actual member. The equivalent mass, stiffness and loading are obtained through out the use of transformation factors to define an equivalent system. Blast design manuals such as TM 5-1300 (Chapter 3) and Biggs 1964 (Chapter 5) contain tabulated transformation factors for typical structural elements and are listed in Appendix B.1. The derivations of the equations for these transformation

factors are also given by these references. Transformation factors used to obtain appropriate properties for the equivalent SDOF system are as follows:

$$\text{Equivalent stiffness, } K_e = K_L K \quad (\text{Equation 6.5a})$$

$$\text{Equivalent mass, } M_e = K_M M \quad (\text{Equation 6.5b})$$

$$\text{Equivalent force, } F_e = K_L F \quad (\text{Equation 6.5c})$$

$$\text{Equivalent resistance, } R_e = K_L R \quad (\text{Equation 6.5d})$$

where,

$$K_L = \quad \text{load or stiffness transformation factor}$$

$$K_M = \quad \text{mass transformation factor}$$

The dynamic analysis can be performed using these equivalent parameters in place of the corresponding actual values. The alternate form of the bilinear dynamic equilibrium equation (Equation 6.4) becomes:

$$M_e a + R_e = F_e \quad (\text{Equation 6.6})$$

Equation 6.6 is simplified through the use of a single load-mass transformation factor,  $K_{LM}$  as follows:

$$K_{LM} M a + K y = F_t, \text{ where} \quad (\text{Equation 6.7})$$

$$K_{LM} = K_M / K_L$$

Transformation factors also change as the structural member progresses from elastic to plastic ranges. The resistance also changes for the plastic range as shown by Equation 6.4. In actual practice, an average of the elastic and plastic transformation factors is used in this case.

Response of construction materials under dynamic loads is governed by the stress-strain relationship. Static mechanical properties are readily available from the variety of sources and are well defined by national codes and standard organizations. Specifications referenced in the codes define minimum properties for various grades of material. In practice, the average strength of materials being installed is approximately 25% greater than the specified minimum values. Therefore a strength increase factor (SIF) is used to account for this condition and is unrelated to strain rate properties of the material. Strength increase factors are used to reduce conservatism and use the full available blast capacity of materials. Blast design manuals such as TM 5-1300 lists SIF factors for various materials as listed in Appendix B.2. A SIF factor of 1.2, the maximum value in the table, is recommended and used in this research program for FRP materials to reduce the huge conservatism when dealing with these new materials.

Construction materials also experience an increase in strength under rapidly applied loads. These materials cannot respond at the same rate as which the load is applied. At a fast strain rate, a greater load is required to produce the same deformation than at a lower rate. To incorporate the effect of material strength increase with strain, a dynamic increase factor (DIF) is applied to static strength values. DIFs are simply ratios of the dynamic material strength to static strength and are a function of material type as well as strain rate. DIFs are also dependent on the type of stress (i.e. flexural, direct shear) because peak values for these stresses occur at different times. Flexural stresses occur very quickly while peak shears occur relatively late in time resulting in a lower strain rate for shear. Blast design manuals such as TM 5-1300 lists DIF factors for various materials as listed in Appendix B.2.

When analyzing elements subjected to shock loads using SDOF systems, a time period between the peak deflections as the element vibrates back and forth is needed. This period is called natural period,  $t_n$ , and is a function of the element's mass and stiffness as illustrated in Equation 6.8.

$$t_n = 2\pi\sqrt{M_e / K}, \text{ where} \quad (\text{Equation 6.8})$$

$M_e$  = equivalent mass

$K$  = stiffness of the SDOF system

Ensuring the adequate response of structural elements to blast loads deformation limits are required. These limits are based on the type of structure or component, construction material used, location of the structure and the desired protection level.

The primary for evaluation of structure response is the evaluation of the ductility ratio and hinge rotations of individual members. Ductility ratio,  $\mu$ , is defined as the maximum displacement of the member divided by the displacement at the elastic limit. It is a measure of the degree of inelastic response experienced by the member. Empirical equations and chart solutions had been derived to estimate the demanded ductility ratio as function of blast load and resistance parameters. [Refer to Appendix B.2 for a chart solution (from TM 5-1300)]. Empirical equations derivations and references are provided from Biggs (1964) and are illustrated in Equations 6.9 to 6.11.

$$\text{If } \tau = (t_d/t_n) < 0.1, \mu_d = 0.5[(2\pi f I_{so}/R_u)^2 + 1] \quad (\text{Equation 6.9})$$

$$\text{If } \tau = (t_d/t_n) > 10, \mu_d = 1/[2(1 - P_{so}/R_u)] \quad (\text{Equation 6.10})$$

In the transition range between these two extreme dynamic responses:

$$P_{so}/R_u = \frac{\sqrt{(2\mu_d - 1)}}{\pi\tau} + \frac{(2\mu_d - 1)\tau}{2\mu_d(\tau + 0.7)} \quad (\text{Equation 6.11})$$

where,

$t_d$  = blast loading time period

$t_n$  = natural period of the SDOF system

$\mu_d$  = demand ductility ratio of the member

$f$  = natural frequency =  $1/t_n$

$I_{so}$  = peak blast impulse

$P_{so}$  = peak blast pressure

$R_u$  = ultimate blast resistance of the SDOF system

Hinge rotations,  $\theta$ , another measure of members response relates the maximum deflection to span and indicates the degree of instability present in critical areas of the members. The angle is formed between a line connecting the endpoints and a line between an endpoint and point of maximum deflection, which is also referred to as support rotation.

Many references such as ASCE Manual 58 and ACI 349 use ductility ratios as the primary gauge of response for concrete and masonry members and treat hinge rotations as secondary criteria for deformation limits. Other references such as TM 5-1300 do not use ductility ratios as deformation limits for concrete and masonry. The relatively stiff nature of concrete and masonry elements produces very high ductility ratios for low maximum deflections. In these cases, ductility ratios may not be indicative of the adequacy of the member and will artificially limit the degree of response. In this manual, hinge rotations are only specified for concrete and masonry elements responding in



flexure and are adopted in this research program. Refer to Appendix B.2 for deformation limits for masonry walls.

**6.3.1. Analysis Study for Un-reinforced Masonry Walls:** The response of un-reinforced walls was predicted based on the assumption that the walls responded as equivalent single-degree-of-freedom system. It was assumed that the failure mode was based on the flexural tensile cracking strength of the masonry, thus the ductility ratio equaled to unity. Tensile cracking strength of masonry is estimated by the Uniform Building Code (1994) guidelines and is illustrated in Equation 6.12.

$$F_r = 2.5\sqrt{f'_m}, \text{ where} \quad (\text{Equation 6.12})$$

$F_r$  : masonry tensile strength (psi)

$f'_m$  : masonry unit prism compressive strength (psi)

The cracking moment was obtained from the equation of elastic materials relationship and it is given as:

$$F_r = \frac{Mc}{I} + \frac{P}{A} \quad (\text{Equation 6.13})$$

Shear capacity is also calculated using Equation 6.1. To obtain the flexural and shear nominal strength of the URM wall, a factor of 2.5 times the allowable stress values from equations 6.1 and 6.12 were taken according to the Building Code Requirements for Masonry Structures 1999. After that, the required resistance of the equivalent SDOF system was computed at a given blast load, and compared with the URM wall's flexural

and shear capacity to check for the walls adequacy to resist the given blast load or its need for retrofit.

### **Validation of Analysis Model for URM Walls**

The analytical model written in a MathCAD program was used to analyze Wall U1 and Wall U2 at different blast pressures reflecting the blast events these walls had been through. Refer to Appendix C.1 for a more detailed analysis of the 4 in. (100 mm) URM wall tested in this research program (Wall U1). Table 6.7 shows the SDOF analysis results for Wall U1 while Table 6.8 shows the SDOF analysis results for Wall U2.

It has been concluded from the results shown in Tables 6.7 and 6.8 that the unreinforced masonry walls of thickness 4 and 8 inches (100 and 203 mm) were governed by their out-of-plane flexural capacity when subjected to blast loads.

Table 6.7 SDOF Analysis Results for Wall U1 at Different Blast Events

<b>Charge (lb*)</b>	<b>Distance (ft**)</b>	<b>Required Resistance (psi**)</b>	<b>+Cracking Flexural Resistance (psi***)</b>	<b>+Required Shear Resistance (psi****)</b>	<b>Maximum Allowable Shear (psi****)</b>
0.5	16	0.38	0.60	3.54	5.4
0.5	12	0.52	0.60	4.30	5.4
1.0	12	0.85	0.60	5.36	5.4
1.5	12	1.13	0.60	6.41	5.4
2.0	12	1.38	0.60	7.45	5.4
3.0	12	1.84	0.60	9.35	5.4
1.5	6	2.53	0.60	28.00	5.4
2.0	6	3.20	0.60	37.00	5.4

\* Convert to Newtons by multiplying by 4.45

\*\* Convert to meters by multiplying by 0.31

\*\*\* Convert to kPa by multiplying by 6.89

<sup>+</sup> Minimum resistance to prevent crack formation

Table 6.8 SDOF Analysis Results for Wall U2 at Different Blast Events

<b>Charge (lb*)</b>	<b>Distance (ft**)</b>	<b><sup>+</sup>Required Resistance (psi***)</b>	<b>Cracking Flexural Resistance (psi***)</b>	<b><sup>+</sup>Required Shear Resistance (psi***)</b>	<b>Maximum Allowable Shear (psi***)</b>
1.0	12	2.60	2.33	7.8	10.94
1.0	8	4.11	2.33	12.6	10.94
1.0	6	5.76	2.33	22.0	10.94
1.5	6	7.40	2.33	30.6	10.94
2.0	6	9.60	2.33	39.0	10.94
3.0	6	13.00	2.33	57.0	10.94
7.5	6	26.10	2.33	134.0	10.94

\* Convert to Newtons by multiplying by 4.45

\*\* Convert to meters by multiplying by 0.31

\*\*\* Convert to kPa by multiplying by 6.89

<sup>+</sup> Minimum resistance to prevent crack formation

Therefore, there is a necessary need to retrofit to URM walls to increase their flexural capacity. It was concluded also that the SDOF approach could be used to predict the URM walls behavior in a conservative manner.

**6.3.2. Analysis Study for FRP Retrofitted Masonry Walls:** The response of FRP retrofitted walls was predicted based on the assumption that the walls responded as equivalent single-degree-of-freedom system and that the vertical (longitudinal) FRP reinforcement acted in a manner similar to steel reinforcement, except that the FRP was a brittle reinforcement. The horizontal FRP reinforcement played a role in increasing the stiffness of the walls retrofitted with them. Since the blast pressure wasn't uniform across the face of the walls and the reinforcement helped in resisting rebound forces based on the observed behavior, however, there was no available data to confirm this. Therefore only vertically FRP retrofitted walls were analyzed using SDOF analysis written in a MathCAD program.

There were two possible failure modes: failure of masonry either in flexure or shear or rupture of FRP. A trial and error approach with several iterations in the program was done to predict the governed failure using equilibrium, compatibility and stress-strain relationships as described below.

$$\alpha\beta_1 = \frac{\varepsilon_m}{\varepsilon'_m} + \frac{-1}{3} \left( \frac{\varepsilon_m}{\varepsilon'_m} \right)^2 \quad (\text{Equation 6.14})$$

$$\alpha\beta_1 \left( 1 - \frac{\beta_1}{2} \right) = \frac{2\varepsilon_m}{3\varepsilon'_m} + \frac{-1}{4} \left( \frac{\varepsilon_m}{\varepsilon'_m} \right)^2 \quad (\text{Equation 6.15})$$

$$\varepsilon_m = \frac{k}{1-k} \varepsilon_f \quad (\text{in case of masonry failure}) \quad (\text{Equation 6.16a})$$

$$\varepsilon_m = \frac{k}{1-k} \varepsilon_{fu} \quad (\text{in case of FRP rupture}) \quad (\text{Equation 6.16b})$$

$$A_f E_f \varepsilon_f = \alpha\beta_1 k t B f'_m \quad (\text{Equation 6.17})$$

$$M_n = \alpha\beta_1 k t f'_m \frac{B}{12} \left( t - \frac{\beta_1}{2} k t \right) \quad (\text{Equation 6.18})$$

where,

$\alpha$  and  $\beta_1$  = equivalent stress block factors used for masonry

$\epsilon_m$  = strain in the masonry

$\epsilon'_m$  = optimum compressive strain in masonry

$\epsilon_f$  = strain in the FRP

$\epsilon_{fu}$  = ultimate strain in FRP

$k$  = ratio factor relating between strain in masonry and FRP

$A_f$  = total area of FRP

$E_f$  = tensile modulus of FRP

$t$  = thickness of masonry wall

$B$  = width of masonry wall

$f'_m$  = compressive strength of masonry

$M_n$  = moment in the system

The above equations were used through some iteration with trial values of  $\alpha$ ,  $\beta_1$  and  $k$  with ultimate masonry and FRP strains in obtaining the actual strains in the masonry and FRP. Then a ratio,  $k_m$  ( $\epsilon_f / \epsilon_{fu}$ ) was calculated. If  $k_m$  was less than 1, then masonry failure governed or vice versa. It was concluded from the analysis, that the failure of masonry always governs the behavior.

After that, the predicted flexural and shear capacities of the reinforced wall were obtained taking into consideration the elastic and plastic behavior of the system and were

compared to the required resistances. Also the maximum deflection, support rotation and ductility ratio of the system were calculated to observe the point of failure according to DOD and Army Code TM 5-1300 requirements.

### **Validation of Analysis Model for FRP Retrofitted Walls**

The analytical model was used to analyze the 4 in. (100 mm) wall vertically reinforced on the backside with three 2.5 in. (63.5 mm) wide GFRP strips [i.e. spacing equal to 9.5 in. (241.3 mm) GFRP sheets (Wall B1) at different blast loads reflecting the blast events these walls had been through. Refer to Appendix C.2 for a more detailed analysis of this wall. Table 6.9 summarizes the single-degree-of-analysis analysis results for Wall B1.

Table 6.9 SDOF Analysis Results for Wall B1 at Different Blast Events

<b>Charge (lb<sup>+</sup>)</b>	<b>Distance (ft<sup>++</sup>)</b>	<b>Maximum Flexural Resistance* (psi<sup>+++</sup>)</b>	<b>Required Shear Resistance** (psi<sup>+++</sup>)</b>	<b>Rotation (degrees)</b>	<b>Maximum Deflection (in)</b>	<b>Ductility Ratio</b>
0.5	16	1.94	3.27	0.20	0.153	0.60
0.25	12	1.93	3.34	0.19	0.145	0.57
0.5	12	1.9	3.74	0.23	0.174	0.70
1.0	12	1.84	4.44	0.33	0.255	1.05
1.5	12	1.90	5.09	0.46	0.355	1.42
2.0	12	1.96	5.72	0.61	0.465	1.81
3.0	12	2.07	7.00	0.91	0.704	2.40
1.5	6	3.15	18.90	1.19	0.900	2.21
2.0	6	3.64	24.00	1.53	1.170	2.46

\* This is compared to the required resistance in Table 6.7

\*\* This is compared to the maximum allowable shear of 5.4 psi as shown in Table 6.7

<sup>+</sup>Convert to Newtons by multiplying by 4.45

<sup>++</sup>Convert to meters by multiplying by 0.31

<sup>+++</sup>Convert to kPa by multiplying by 6.89

The analytical results shown in Table 6.9 matched with the actual response of Wall B1, as the wall was governed by its shear capacity when subjected to blast loads. Therefore, increasing the out-of-plane flexural capacity of URM walls has to be associated with proper wall to frame connections with increasing the shear capacity by grouting the wall or reducing span length to resist higher shear stresses and transfer the rebound forces resulted from the retrofit or else the retrofitted wall blast capacity will reduce, as the reinforced wall's shear capacity controls.

Wall B1 deflected 0.153 in. (3.89 mm) at event #1; the same amount of deflection resulted from the analytical approach. There are no other available data, but it seems that the SDOF approach could estimate the maximum deflections with high accuracy especially in the elastic range of the walls.

Support rotations computed from the SDOF analysis, a deflection limit for masonry walls adapted by the Department of Defense and the Army Code TM 5-1300 (Refer to Appendix B.2), reflected the actual behavior with the threat and damage levels facing Wall B1 as illustrated in Table 6.10. Therefore a value of 0.5 degrees or less of support rotation reflected a minimum or low threat level with no damage, while a support rotation value between 0.5 to 0.75 degrees reflected a medium threat level with no or low

damage. The range of 0.75 to 1 degrees of support rotation reflected a high threat level with heavy shear damage, and a support rotation above 1 degree reflected high threat level with collapse failure.

Table 6.10 Damage and Threat Levels vs. Rotation and Ductility Ratios for Wall B1

<b>Charge (lb*)</b>	<b>Standoff Distance (ft**)</b>	<b>Damage Level</b>	<b>Threat Level</b>	<b>Rotation (degrees)</b>	<b>Ductility</b>
0.5	16	No Damage	Minimum	0.20	0.60
0.5	12	No Damage	Low	0.23	0.70
1.0	12	No Damage	Low	0.33	1.05
1.5	12	No Damage	Medium	0.46	1.42
2.0	12	Light Damage	Medium	0.61	1.81
3.0	12	Heavy Damage (Shear Damage)	High	0.91	2.40
2.0	6	Failure (Flexural)	High	1.53	2.21

\*Convert to Newtons by multiplying by 4.45

\*\*Convert to meters by multiplying by 0.31

The ductility ratio could be also correlated to the damage level facing Wall B1 as illustrated in Table 6.10. This approach exists in some references and sponsored by some researchers for additional blast design guidelines (refer to Section 2.2.2 and Equation 2.1). A ductility ratio of 1.0 or less reflected a minimum or low threat level with no damage, while between 1.0 to 1.5 reflected a medium threat level with no damage while a ductility ratio between 1.5 to 2.0 reflected a medium threat level with light damage. A



ductility ratio above 2.0 reflected high threat level with heavy shear damage or collapse failure.

Therefore, it was concluded that the SDOF approach that is commonly used to predict the blast response of structural elements can be used to predict the blast response of URM walls retrofitted with FRP.

It was also concluded when comparing of the calculated support rotations and ductility ratios with the test results and the observed damages for the walls has provided some guidelines when retrofitting masonry walls with FRP as shown in the tables below.

Table 6.11 Support Rotation Guidelines for FRP Strengthened Walls

<b>Support Rotation (degrees)</b>	<b>Threat Level</b>	<b>Damage Level</b>
< 0.5	Minimum or Low	No damage
0.5-0.75	Medium	No or low damage
0.75-1.0	High	Heavy damage (shear)
>1.0	High	Failure (flexural collapse)

Table 6.12 Ductility Ratio Guidelines for FRP Strengthened Walls

<b>Ductility Ratio</b>	<b>Threat Level</b>	<b>Damage Level</b>
< 1.0	Minimum or Low	No damage
1.0-1.5	Medium	No damage
1.5-2.0	Medium	Low damage
>2.0	High	Heavy damage (shear) or Failure (flexural collapse)

## **7. CONCLUSIONS AND RECOMMENDATIONS FOR FUTURE RESEARCH**

### **7.1. CONCLUSIONS**

This research program has demonstrated that FRP composites offer great benefits for the strengthening of masonry walls to resist blast loads. FRP systems have been proven to increase remarkably the out-of-plane flexure capacity of URM elements to resist more blast threat levels, but it has to be associated with proper shear capacity and wall to frame connections, as the strengthened wall's shear capacity controls.

It has also been shown that failure of the FRP strengthened walls have failed in a safe manner controlling their debris. Shear damage or failure in a stable manner gave an indication for not surviving additional blast loads. If additional blast loads were applied, the retrofitted walls' collapsed towards the outside direction in contact debris that would help in reducing the hazard of causing possible harm and injury to building occupants while the un-reinforced walls failed in a sudden flexural manner towards the inside direction with scattered debris.

The test results also showed that the SDOF approach that is commonly used to predict the blast response of structural components can be used to predict the blast response of URM walls strengthened vertically on the backside with FRP.

A comparison of the calculated support rotations and ductility ratios with the test results and the observed damages for the walls and comparing them with the DOD and TM 5-1300 Code requirements (Refer to Tables 4.1, 4.2 and B.2.3), has provided some guidelines when retrofitting masonry walls with FRP as shown in the Tables 6.11 and 6.12.

## 7.2. FUTURE RECOMMENDATIONS

The following recommendations for future work are suggested:

- Investigation on type of connections and the interaction of strengthened walls with the surrounding structural elements (i.e. beams and columns) since the effectiveness of the strengthening against blast loads depends on the transfer of rebound forces of these walls.
- Investigation on improving shear capacity of FRP retrofitted masonry walls to resist high shear stresses and rebound forces from high blast loads. Grouting the walls or reducing span length are some recommended techniques.
- For the development of design protocols for the flexural strengthening of URM walls under blast loads, different FRP reinforcement ratios need to be studied to observe its influence in different modes of failure such as masonry flexure or shear failure or FRP rupture. Other variables to be studied should include different types of FRP materials, hybrid systems of FRP and concrete grouting, both face strengthening of the walls, different and representative types of masonry units, effect of wall openings on blast capacity, and different wall slenderness and height to width ratios.
- For masonry walls strengthened by FRP structural repointing in the horizontal direction, more research needs to be conducted to investigate the effectiveness and contribution of such reinforcement on the blast capacity of masonry walls with varying boundary conditions and connection details.

- For the validation needed for peak pressure determination, more experimental blast work needs to be conducted with different charge types, weights and different standoff distances. Other variables to be studied should include blast wave interaction facing different sides of a building, vacuum pressures and ground vibration.

**APPENDIX A.**  
**PRESSURE AND DEFLECTION RESULTS**

### A.1 PRESSURE AND DEFLECTION PROFILES

The Figures listed below represent the typical pressure and deflection profiles obtained by the instrumentation at different blast levels.

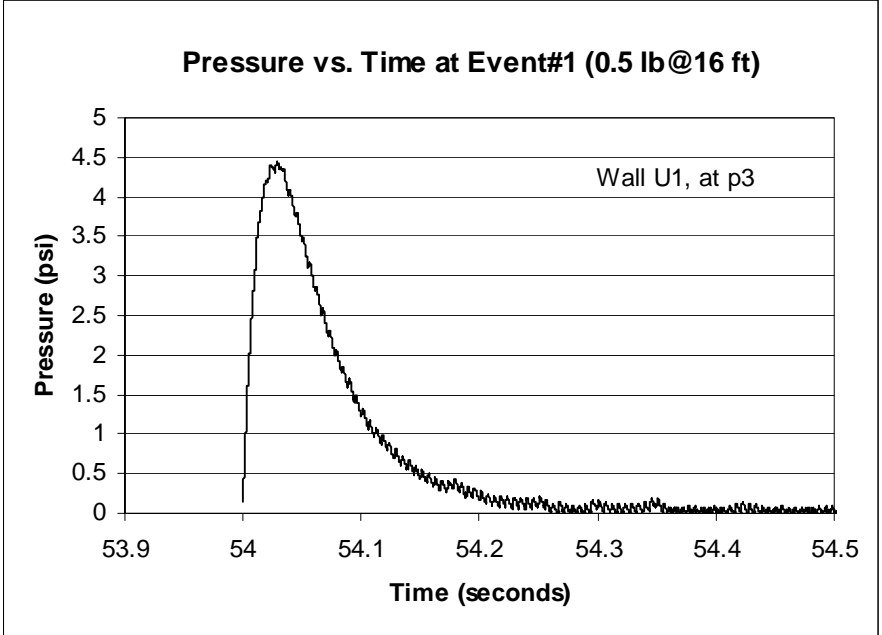


Figure A.1.1 Pressure Wave vs. Time at 0.5 lb @ 16ft for Wall U1 at p3

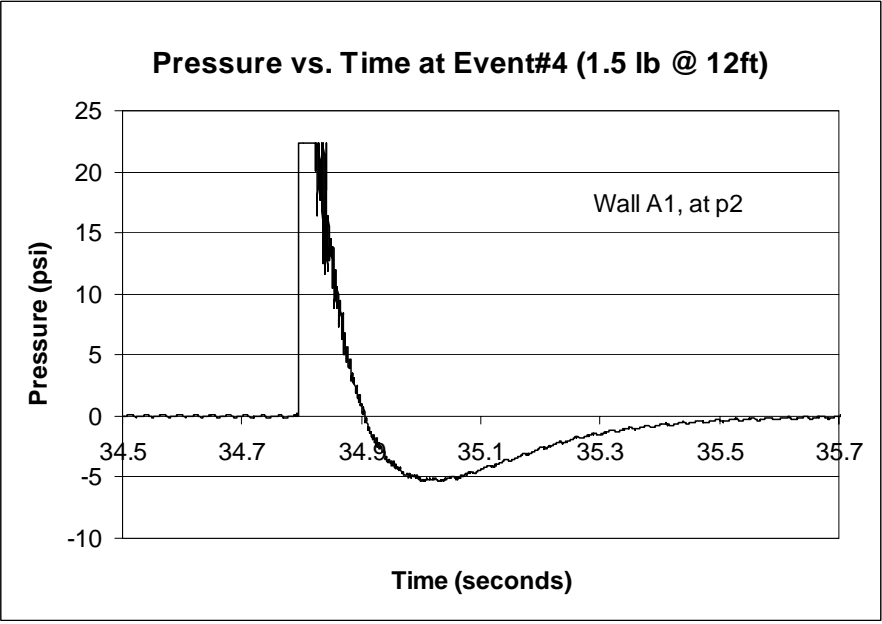


Figure A.1.2 Pressure Wave vs. Time at 1.5 lb @ 12ft for Wall A1 at p2

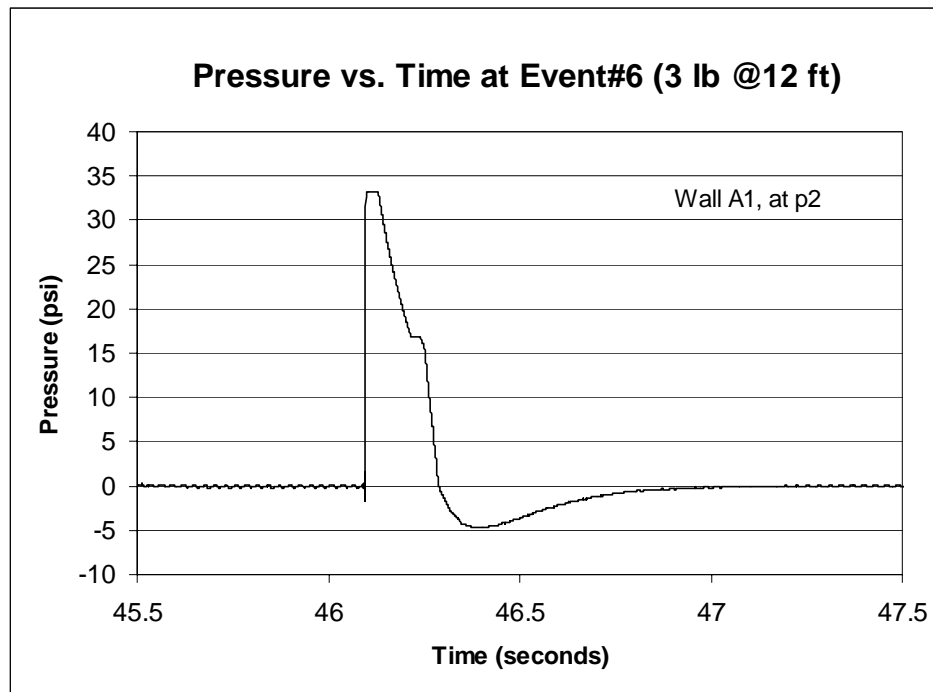


Figure A.1.3 Pressure Wave vs. Time at 3.0 lb @ 12ft for Wall A1 at p2

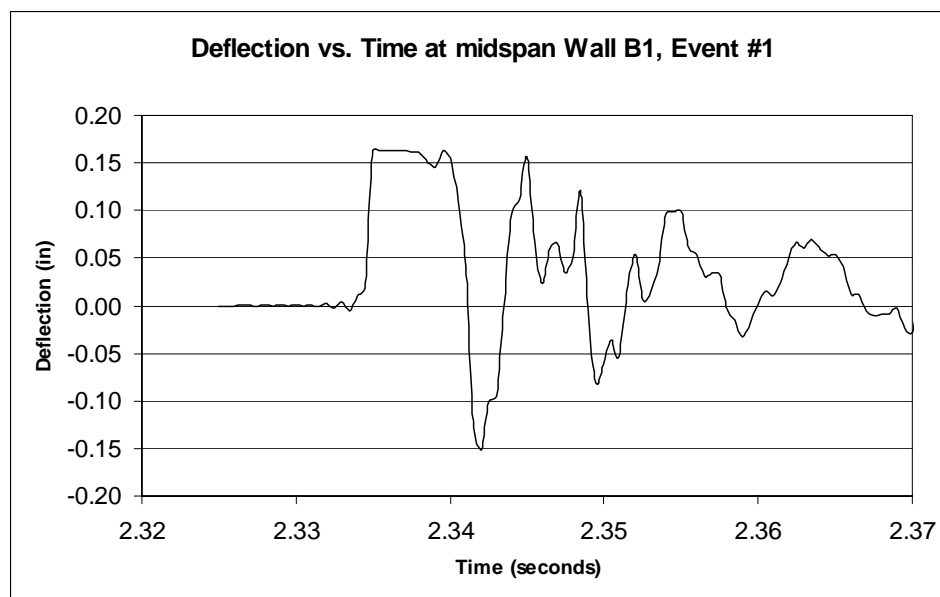


Figure A.1.4 Mid-span Deflection Wave vs. Time at 0.5 lb @ 16ft for Wall B1

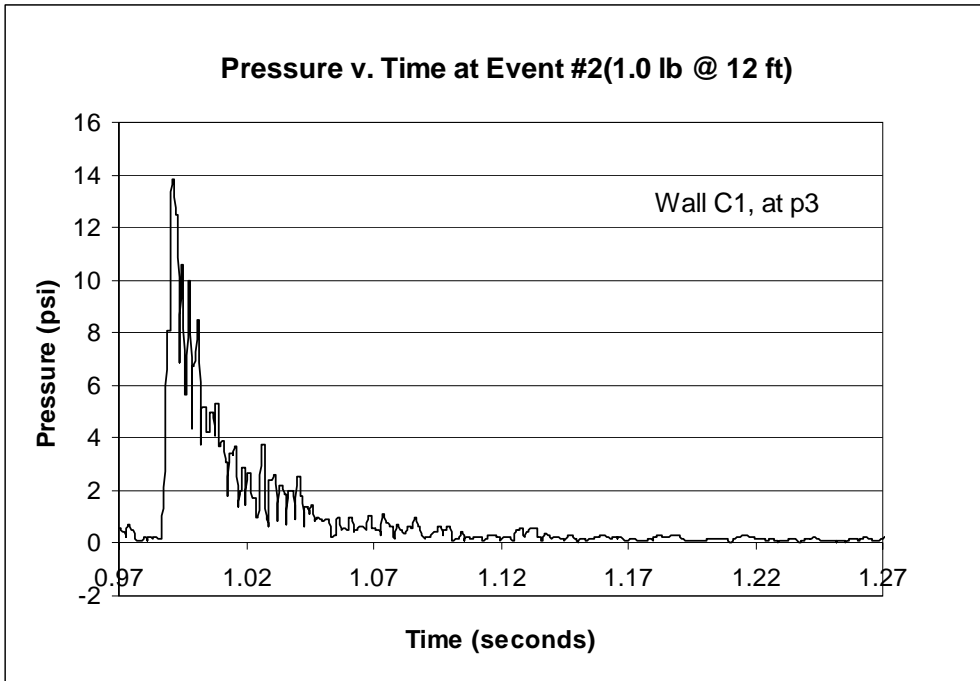


Figure A.1.5 Pressure Wave vs. Time at 1.0 lb @ 12ft for Wall C1 at p3

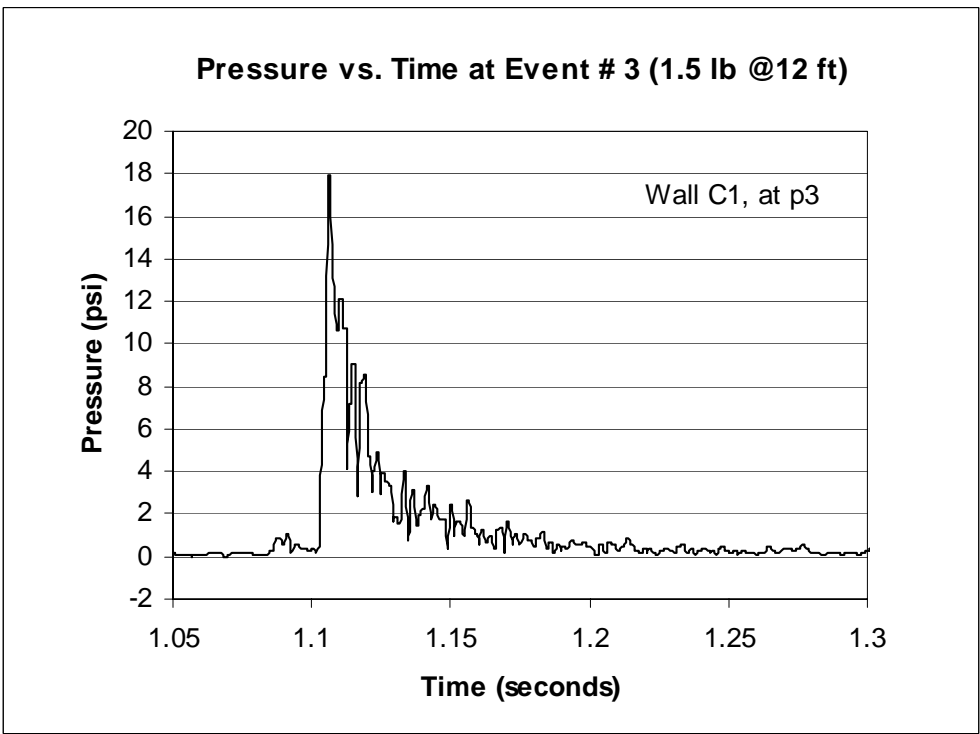


Figure A.1.6 Pressure Wave vs. Time at 1.5 lb @ 12ft for Wall C1 at p3



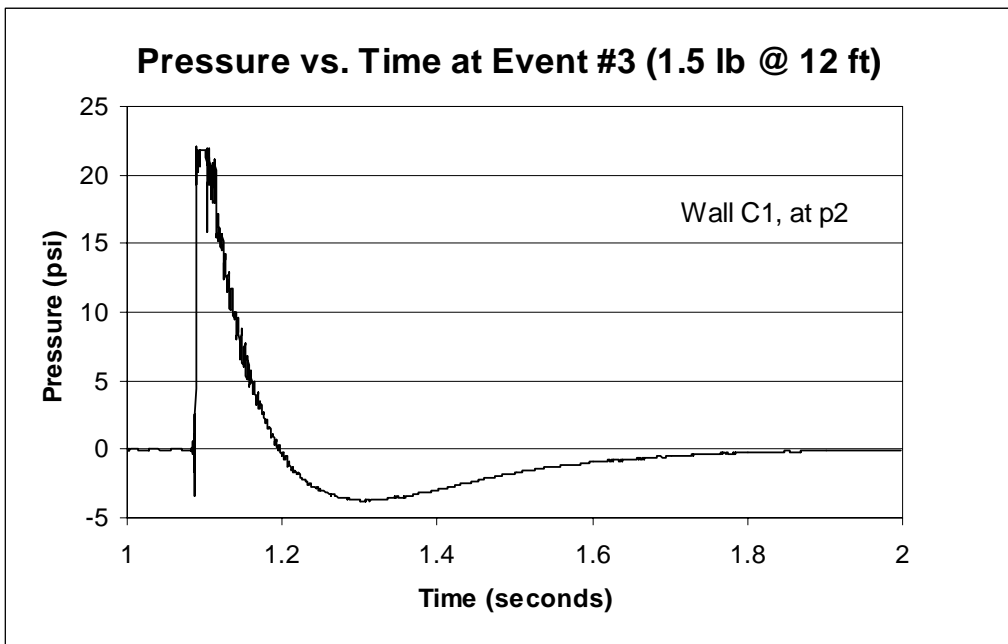


Figure A.1.7 Pressure Wave vs. Time at 1.5 lb @ 12ft for Wall C1 at p2

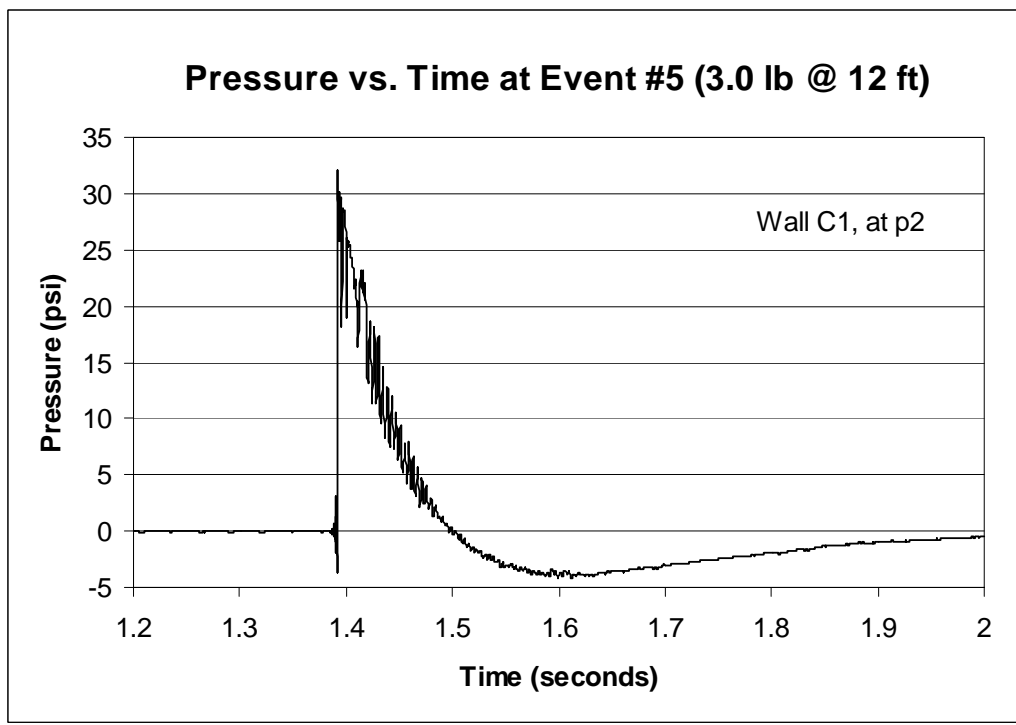


Figure A.1.8 Pressure Wave vs. Time at 3.0 lb @ 12ft for Wall C1 at p2

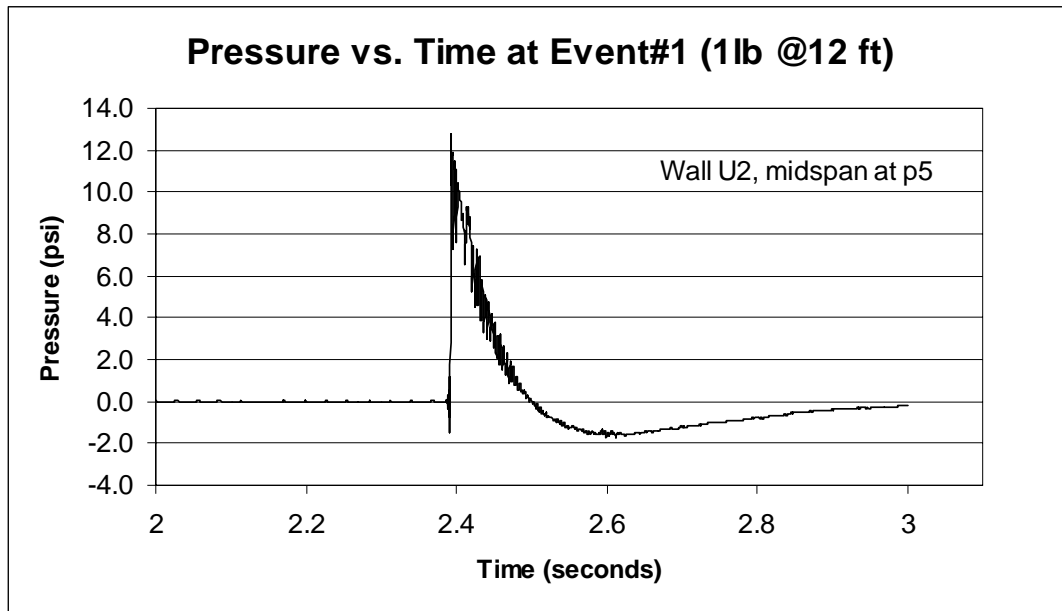


Figure A.1.9 Pressure Wave vs. Time at 1.0 lb @ 12ft for Wall U2 at p5

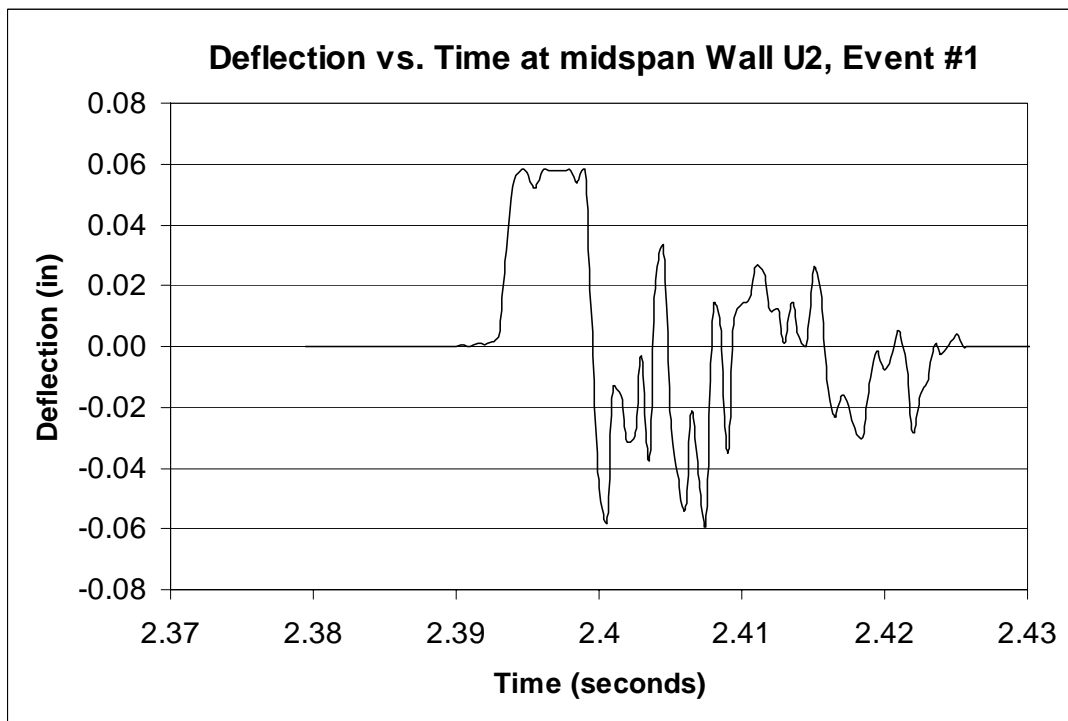


Figure A.1.10 Mid-span Deflection Wave vs. Time at 1.0 lb @ 12ft for Wall U2

## A.2 EXPERIMENTAL VS. THEOROTICAL PRESSURES VALUES

The tables listed below represent the experimental blast pressure values obtained at different blast levels at different locations on the wall versus the theoretical values obtained from Model 1 at same positions and events.

Table A.2.1 Experimental and Theoretical Peak Pressure Values at Test Wall # 1 (U1)

		Peak Pressure (psi *)									
		P2		P3		P4		P5		P6	
Charge (lb)	Distance (ft)	Model 1	Experiment.	Model 1	Experiment.	Model 1	Experiment.	Model 1	Experiment.	Model 1	Experiment.
0.25	16	4.44	3.5	4.46	3.35	4.42	3.51	4.52	4.1	4.35	3.46
0.5	16	6.25	5.78	6.28	5.99	6.22	6.01	6.4	8.9	6.11	6.1
0.5	12	9.96	10.01	10.03	10.1	9.83	8.4	10.35	11.5	9.52	8.2
1.0	8	39.39	38.25	40.42	42.45	37.8	35.23	41.37	46.9	34.2	34

Table A.2.2 Experimental and Theoretical Peak Pressure Values at Test Wall # 2 (A1)

		Peak Pressure (psi *)							
		P2		P4		P5		P6	
Charge (lb)	Distance (ft)	Model 1	Experiment.	Model 1	Experiment.	Model 1	Experiment.	Model 1	Experiment.
0.25	20	4.24	3.24	4.23	3.27	4.29	5.40	4.19	3.75
0.25	16	5.77	-----	5.75	-----	5.88	5.30	5.66	-----
0.25	12	6.80	-----	6.72	-----	7.00	7.20	6.52	-----
0.50	12	12.95	9.30	12.78	9.96	13.46	15.50	12.38	9.50
0.75	12	16.64	-----	16.41	-----	17.30	15.60	15.81	-----
1.00	12	20.22	-----	19.90	-----	20.97	22.00	19.15	-----
1.50	12	20.88	22.00	20.54	15.60	21.54	24.50	19.69	16.30
2.00	12	26.12	-----	25.67	-----	26.85	28.50	24.57	-----
3.00	12	36.36	32.60	35.68	29.30	37.40	35.80	34.03	30.70

Table A.2.3 Experimental and Theoretical Peak Pressure Values at Test Wall # 3 (B1)

		Peak Pressure (psi *)									
		P2		P3		P4		P5		P6	
Charge (lb)	Distance (ft)	Model 1	Experiment.	Model 1	Experiment.	Model 1	Experiment.	Model 1	Experiment.	Model 1	Experiment.
0.5	12	9.96	9.6	10.03	13.73	9.83	12.13	10.35	17	9.52	12.5

Table A.2.4 Experimental and Theoretical Peak Pressure Values at Test Wall # 4 (C1)

		Peak Pressure (psi *)									
		P2		P3		P4		P5		P6	
Charge (lb)	Distance (ft)	Model 1	Experiment.	Model 1	Experiment.	Model 1	Experiment.	Model 1	Experiment.	Model 1	Experiment.
0.5	12	9.96	9.74	10.03	9.23	9.83	8.4	10.35	11.8	9.52	9.54
1.0	12	15.55	13.78	15.69	13.84	15.31	13.42	16.13	17.3	14.73	13.6
1.5	12	20.88	21.76	21.08	18.1	20.54	20.45	21.54	22.37	19.69	18.54
2.0	12	26.12	24	26.37	26.5	25.67	22.5	26.85	27.5	24.57	22.3
3.0	12	36.36	31.7	36.75	31.8	35.68	33	37.40	35.4	34.03	31.3

Table A.2.5 Experimental and Theoretical Peak Pressure Values at Test Wall # 6 (U2)

		Peak Pressure (psi *)									
		P2		P3		P4		P5		P6	
Charge (lb)	Distance (ft)	Model 1	Experiment.	Model 1	Experiment.	Model 1	Experiment.	Model 1	Experiment.	Model 1	Experiment.
1.0	12	15.55	15.5	15.69	17.03	15.31	14.28	16.13	13.2	14.73	12.88
1.0	8	39.39	38.2	40.42	38.7	37.8	38.9	41.37	40.4	34.2	31.7
1.0	6	84.1	83.7	88.15	80.6	78.2	70.8	91.48	93.8	65.22	61.54
1.5	6	124.99	117	131.38	131	115.71	107.6	136.33	136.8	95.33	96.6

Table A.2.6 Experimental and Theoretical Peak Pressure Values at Test Wall # 7 (A2)

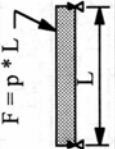
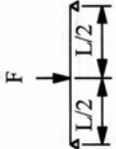
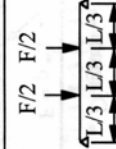
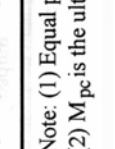


		Peak Pressure (psi *)									
		P2		P3		P4		P5		P6	
Charge (lb)	Distance (ft)	Model 1	Experiment.	Model 1	Experiment.	Model 1	Experiment.	Model 1	Experiment.	Model 1	Experiment.
1.0	12	15.55	15.54	15.69	15.3	15.31	15.1	16.13	20.3	14.73	14.6
1.0	8	39.39	37.85	40.42	41.76	37.8	38.8	41.37	44.2	34.2	38.5
1.0	6	84.1	76.3	88.15	79.7	78.2	81.2	91.48	113	65.22	68.3

**APPENDIX B.**  
**BLAST ANALYSIS; FACTORS, EQUATIONS AND REQUIREMENTS**

## B.1 SDOF ANALYSIS; FACTORS AND EQUATIONS

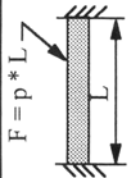
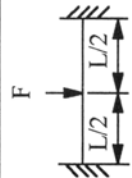
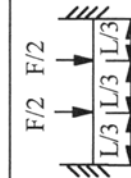
Blast design manual TM 5-1300 (Chapter 3) contains the tables shown below that represent different SDOF systems with their transformation factors, stiffness constants, bending resistance and dynamic reactions.

Table B.1.1 Transformation Factors, for Simply Supported Members

Loading Diagram	Strain Range	Load Factor $K_L$	Lumped Mass Factor, $K_M(1)$	Uniform Mass Factor, $K_M$	Bending Resistance, $R_b$	Spring Constant, K	Dynamic Reaction, V
	Elastic	0.64	---	0.50	$8M_{pc}/L$	$384 EI/5L^3$	$0.39R_u + 0.11F$
	Plastic	0.50	---	0.33	$8M_{pc}/L$	0	$0.38R_u + 0.12F$
	Elastic	1.00	1.00	0.49	$4M_{pc}/L$	$48 EI/L^3$	$0.78R_u - 0.28F$
	Plastic	1.00	1.00	0.33	$4M_{pc}/L$	0	$0.75R_u - 0.25F$
	Elastic	0.87	0.76	0.52	$6M_{pc}/L$	$56.4 EI/L^3$	$0.525R_u - 0.025F$
	Plastic	1.00	1.00	0.56	$6M_{pc}/L$	0	$0.52R_u - 0.02F$

Note: (1) Equal portions of the concentrated mass are lumped at each concentrated load.  
 (2)  $M_{pc}$  is the ultimate moment capacity at midspan.

Table B.1.2 Transformation Factors, for Fixed Supported Members

Loading Diagram	Strain Range	Load Factor $K_L$	Lumped Mass Factor, $K_M(1)$	Uniform Mass Factor, $K_M$	Bending Resistance, $R_b$	Spring Constant, K	Dynamic Reaction, V
	Elastic E-P (2) Plastic	0.53 0.64 0.50	--- --- ---	0.41 0.50 0.33	$12M_{ps}/L$ $8(M_{ps}+M_{pc})/L$ $8(M_{ps}+M_{pc})/L$	$384 EI/L^3$ $384 EI/5L^3$ 0	$0.36R + 0.14F$ $0.39R + 0.11F$ $0.38R_u + 0.12F$
	Elastic Plastic	1.00 1.00	1.00 1.00	0.37 0.33	$4(M_{ps}+M_{pc})/L$ $4(M_{ps}+M_{pc})/L$	$192 EI/L^3$ 0	$0.71R - 0.21F$ $0.75R_u - 0.25F$
	Elastic Plastic	0.87 1.00	0.76 1.00	0.52 0.56	$6M/L$ $6M/L$	$56.4 EI/L^3$ 0	$0.53R - 0.03F$ $0.52R_u - 0.02F$

Note: (1) Equal portions of the concentrated mass are lumped at each concentrated load.

(2) E-P is Elastic-Plastic.

(3)  $M_{pc}$  is the ultimate moment capacity at midspan;  $M_{ps}$  is the ultimate moment capacity at support.



Table B.1.3 Transformation Factors, for Simple-Fixed Supported Members

Loading Diagram	Strain Range	Load Factor $K_L$	Lumped Mass Factor, $K_M(1)$	Uniform Mass Factor, $K_M$	Bending Resistance, $R_b$	Spring Constant, K	Dynamic Reaction, V
	Elastic E-P (2) Plastic	0.58 0.64 0.50	--- --- ---	0.45 0.50 0.33	$8M_{pc}/L$ $4(M_{ps} + 2M_{pc})/L$ $4(M_{ps} + 2M_{pc})/L$	$185 EI/L^3$ $384 EI/5L^3$ 0	$V1 = 0.26R + 0.12F$ $V2 = 0.43R + 0.19F$ $0.39R + 0.11F \pm M_{ps}/L$ $0.38R_u + 0.12F \pm M_{ps}/L$
	Elastic E-P Plastic	1.00 1.00 1.00	1.00 1.00 1.00	0.43 0.49 0.33	$16M_{pc}/3L$ $2(M_{ps} + 2M_{pc})/L$ $2(M_{ps} + 2M_{pc})/L$	$107 EI/L^3$ $48 EI/L^3$ 0	$V1 = 0.25R + 0.07F$ $V2 = 0.54R + 0.14F$ $0.78R - 0.28F \pm M_{ps}/L$ $0.75R_u - 0.25F \pm M_{ps}/L$
	Elastic E-P Plastic	0.81 0.87 1.00	0.67 0.76 1.00	0.45 0.52 0.56	$6M_{pc}/L$ $2(M_{ps} + 3M_{pc})/L$ $2(M_{ps} + 3M_{pc})/L$	$132 EI/L^3$ $56 EI/L^3$ 0	$V1 = 0.17R + 0.17F$ $V2 = 0.33R + 0.33F$ $0.525R - 0.025F \pm M_{ps}/L$ $0.52R_u - 0.02F \pm M_{ps}/L$

Notes: (1) Equal portions of the concentrated mass are lumped at each concentrated load.  
(2) E-P is Elastic - Plastic.  
(3)  $M_{pc}$  is the ultimate moment capacity at midspan;  $M_{ps}$  is the ultimate moment capacity at support.

## B.2 BLAST ANALYSIS; MATERIAL STRENGTH AND RESPONSE CRITERIA

Blast design manual TM 5-1300 (Chapter 3) contains the tables and requirements shown below for dynamic material strength (SIF and DIF factors) and response criteria of masonry (support rotation limits, and ductility graphical solutions).

Table B.2.1 Strength Increase Factors (SIF)

Material	SIF
Structural Steel ( $f_y \leq 50$ ksi)	1.10
Reinforcing Steel ( $f_y \leq 60$ ksi)	1.10
Cold-formed Steel	1.21
Concrete and Masonry	1.00

Table B.2.2 Dynamic Increase Factors (DIF)

Stress Type	DIF			
	Reinforcing Bars		Concrete	Masonry
	$F_{dy}/F_y$	$F_{du}/F_u$	$f'_{dc}/f'_c$	$f'_{dm}/f'_m$
Flexure	1.17	1.05	1.19	1.19
Compression	1.10	1.00	1.12	1.12
Diagonal Tension	1.00	1.00	1.00	1.00
Direct Shear	1.10	1.00	1.10	1.00
Bond	1.17	1.05	1.00	1.00

Table B.2.3 Deformation Limits for Masonry (TM 5-1300)

Element Type	Support Rotation, $\theta$ (degrees)		
	Low Threat Level	Medium Threat Level	High Threat Level
One-way	0.50	0.75	1.00
Two-way	0.50	1.00	2.00

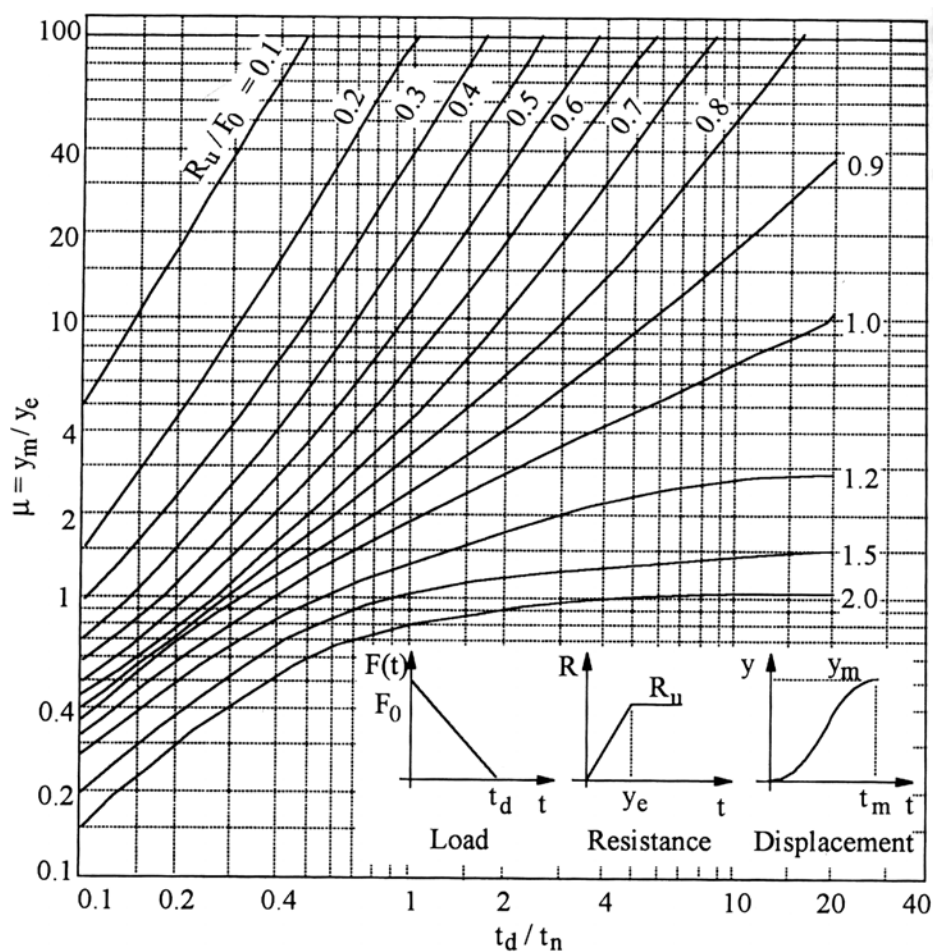


Figure B.2.1 Graphical Solution Chart for SDOF System (TM 5-1300)

**APPENDIX C.**  
**SINGLE-DEGREE-OF-FREEDOM DETAILED ANALYSIS**

### C.1 SDOF ANALYSIS FOR UN-REINFORCED MASONRY WALL (WALL U1)

The response of one-way un-reinforced masonry walls was predicted based on the assumption that the walls responded as equivalent single-degree-of-freedom system. It was assumed that the failure mode was based on the flexural tensile cracking strength of the masonry, thus the ductility ratio equaled to unity ( $\mu_d = 1.0$ ).

*Properties of Wall U1 (Masonry Designers' Guide, 2001):*

Hollow masonry compressive strength,  $f'_m = 1500$  psi (10.34 MPa)

Actual thickness,  $t = 3.625$  in (9.21 cm)

Area,  $A = 18.0$  in<sup>2</sup>/ft of wall (381 cm<sup>2</sup>/m)

Moment of inertia,  $I_g = 38.0$  in<sup>4</sup>/ft of wall (5189.24 cm<sup>4</sup>/m)

Density of masonry unit = 110 pcf (1762.03 kg/m<sup>3</sup>)

*Dimensions of Wall U1:*

Wall Height,  $L = 88$  in (223.52 cm)

Wall Width,  $B = 48$  in (121.92 cm)

*Blast Load:*

This un-reinforced wall is evaluated at a blast threat of 1 lb (4.45 N) of Pentolite at a standoff distance of 12 ft (3.66 m) from center of wall.

The blast pressure and duration taken from actual data reading and can be determined from the empirical relation developed in this report (Refer to Equation 5.1) or from Model 1 (Refer to Section 2.1.1).

Therefore, the blast peak pressure,  $P_{so} = 16.13$  psi (111.21 kPa)

Effective duration,  $t_d = 1.83$  ms

Impulse,  $I_{so} = 14.77$  psi-ms (101.84 psi-ms)

Wall U1 is a one-way un-reinforced wall because of high slenderness ratio ( $L/t = 22$ ) and low wall height to width ratio ( $L/B = 1.83$ ). The boundary conditions of wall U1 are fixed from top support carrying a beam of 200 lb (889.64 N) and simply supported from the bottom and free on the edges. The analysis is in the elastic range since  $\mu_d = 1$ .

Computing Required Flexural Resistance: (based on unit inch width of the wall)

For dynamic flexure, (Refer to Tables B.2.1 and B.2.2)

$$\begin{aligned} f'_{dm} &= (\text{SIF})(\text{DIF}) f'_m \\ &= (1.00)(1.19)(1500) = 1785 \text{ psi (12.3 MPa)} \end{aligned}$$

Modulus of Elasticity, (Building Code Requirements of Masonry Structures)

$$\begin{aligned} E_m &= 900 f'_{dm} \\ &= 900(1785) = 1,606,500 \text{ psi} = 1606.5 \text{ ksi (11076.43 MPa)} \end{aligned}$$

Effective Stiffness, (Refer to Table B.1.3)

$$\begin{aligned} K &= 185E_m I_g/L^3 \\ &= 185(1606.5)(38.0/12)/(88^3) = 1.38 \text{ k/in} = 15.69 \text{ psi/in (43.27 kPa/cm)} \end{aligned}$$

Weight of Wall,

$$\begin{aligned} \text{Weight} &= \text{Density (A)(L)} \\ &= (110)(18/1728)(88/12) = 8.4 \text{ lb} = 0.095 \text{ psi (0.67 kPa)} \end{aligned}$$

Compute Mass,

$$\begin{aligned} M &= \text{Weight/gravity} \\ &= [0.095 + (200/88)]/(386) = 0.006135 \text{ psi-sec}^2/\text{in} \\ &= 6135 \text{ psi-ms}^2/\text{in (16,653 kPa-ms}^2/\text{cm)} \end{aligned}$$

Since in elastic range response, use elastic values for  $K_{LM}$  (Refer to Table B.1.3)

$$K_{LM} = K_M/K_L = 0.45/0.58 = 0.776$$

Equivalent mass,

$$M_e = (K_{LM})(M) = (0.776)(6135) = 4760 \text{ psi-ms}^2/\text{in} \text{ (12920.67 kPa-ms}^2/\text{cm)}$$

Natural period,

$$t_n = 2\pi\sqrt{M_e / K} = 2\pi\sqrt{4760/15.69} = 109.43 \text{ ms}$$

Duration-Period ratio,

$$\tau = t_d/t_n = 1.83/109.43 = 0.017$$

Since,  $\tau = 0.017 < 0.1$ , Therefore use Equation 6.9

$$\text{Therefore, } \mu_d = 0.5[(2\pi f_{so}/R_m)^2 + 1]$$

$$\text{Therefore, } R_m = \frac{2\pi I_{so}}{t_n \sqrt{(2\mu_d) - 1}} = \frac{2\pi(14.77)}{(109.43)\sqrt{2(1) - 1}} = 0.848 \text{ psi (5.85 kPa)}$$

Therefore, required flexural resistance,  $R_m = 0.848 \text{ psi (5.85 kPa)}$

Available Flexural Capacity: (based on unit inch width of the wall)

Since flexure is based on cracking strength of masonry, then use Equation 6.12 multiplying by 2.5 to obtain nominal strength.

Modulus of rupture,

$$F_r = 2.5(2.5\sqrt{f'_{dm}}) = 2.5(2.5\sqrt{1785}) = 264.06 \text{ psi (1820.63 kPa)}$$

Weight of wall above mid-height,

$$W_m = (0.095)(88/2) + 200/(88/2) = 104.20 \text{ lb (463.50 N)}$$

Computing cracking moment, (Refer to Equation 6.13)

$$M_{cr} = (F_r + W_m/A)I_g / (0.5t) = [264.06 + 104.2 / (18/12)](38/12) / [(0.5)(3.625)]$$

$$= 582.71 \text{ lb.in (6583.57 N.cm)}$$

Resistance at cracking moment, (Refer to Table B.1.3)

$$R_b = 8M_{cr}/L = 8(582.71)/(88) = 52.97 \text{ lb (235.62 N)}$$

Therefore, flexural unit resistance,  $R_{ub} = 52.97/(88)(1) = 0.602 \text{ psi (4.15 kPa)}$

Computing Available Shear Capacity: (based on unit inch width of the wall)

For dynamic shear, (Refer to Tables B.2.1 and B.2.2)

$$f'_{dm} = (\text{SIF})(\text{DIF}) f'_m$$

$$= (1.0)(1.0)(1500) = 1500 \text{ psi (10.3 MPa)}$$

Obtain shear capacity using Equation 6.1 and multiplying it by 2.5 to obtain the nominal shear strength,

$$V_n = 2.5(1.5A\sqrt{f'_{dm}}) = 2.5[1.5(18/12)\sqrt{1500}] = 217.86 \text{ lb (969.10 N)}$$

The critical section for shear is a distance  $t$  from the top support,

$$R_s = V_n L / (0.5L - t) = 217.86(88) / [(0.5)(88) - 3.625] = 474.83 \text{ lb (2112.15 N)}$$

Therefore, shear unit resistance,  $R_{us} = 474.83/(88)(1) = 5.4 \text{ psi (37.23 kPa)}$

Computing Required Shear Resistance: (based on unit inch width of the wall)

Maximum shear force (reaction) in system (Refer to Table B.1.3)

$$V_o = 0.43R_s + 0.19 P_{so}L = 0.43(474.83) + 0.19(16.13)(88)(1)$$

$$= 473.87 \text{ lb (2107.88 N)}$$

Therefore, required shear resistance,  $V_{uo} = 473.87/(88)(1) = 5.38 \text{ psi (37.10 kPa)}$



## Conclusion

Since  $V_{uo} < R_{us}$ , therefore wall has no problem with shear.

Since  $R_{ub} < V_{uo}$ , therefore bending controls the wall behavior.

Therefore, the maximum capacity of wall U1,  $R_u = R_{ub} = 0.602$  psi (4.15 kPa) but the required flexural resistance,  $R_m = 0.848$  psi (5.85 kPa).

Therefore, the un-reinforced wall U1 only provides 71% of the required resistance for the specified blast load. For adequate resistance, the existing wall must either be strengthened, or a new wall must be added next to the existing wall.

Appendix C.2 provides the detailed analysis a wall with the same properties of Wall U1 strengthened with vertical FRP sheets.

## C.2 SDOF ANALYSIS FOR FRP REINFORCED MASONRY WALL (WALL B1)

The response of FRP retrofitted masonry wall B1 was predicted based on the assumption that the walls responded as equivalent single-degree-of-freedom system and that the vertical FRP reinforcement acted in a manner similar to steel reinforcement, except that the FRP was a brittle reinforcement. It was assumed two possible failure modes: failure of masonry or rupture of FRP.

As concluded from Appendix C.1, the un-reinforced wall U1 must be strengthened in flexure for adequate resistance at the mentioned blast threat. Therefore, the un-reinforced wall was retrofitted vertically with three 2.5 in (63.5 mm) wide GFRP strips (i.e. spacing equal to 9.5 in (241.3 mm)) presented in wall B1.

Wall B1 had the same properties and dimensions of Wall U1, and this wall was also evaluated at the same blast threat.

### *Properties of GFRP Sheets:*

Area per sheet = 0.12 in<sup>2</sup> (0.774 cm<sup>2</sup>) and Number of sheets = 3

Therefore, total fiber area,  $A_f = (0.12)(3) = 0.36 \text{ in}^2$  (2.32 cm<sup>2</sup>)

Center to center spacing,  $S = 12 \text{ in}$  (30.48 cm)

GFRP tensile strength,  $f'_{fu} = 240 \text{ ksi}$  (1654.74 MPa)

GFRP tensile modulus,  $E_f = 12,000 \text{ ksi}$  (82737.09 MPa)

For dynamic flexure, (Refer to Section 6.3, Tables B.2.1 and B.2.2)

$$\begin{aligned} f'_{dfu} &= (\text{SIF})(\text{DIF}) f'_{fu} \\ &= (1.3)(1.05)(240) = 327.6 \text{ ksi (2258.72 MPa)} \end{aligned}$$

$$\begin{aligned} \text{Therefore, } \varepsilon_{fu} &= f'_{dfu}/E_f \\ &= 327.6/12,000 = 0.0273 \text{ (ultimate strain in GFRP sheet)} \end{aligned}$$

Two possible failures: masonry failure or FRP rupture. A trial and error approach with several iterations was done to predict the governed failure using equilibrium, compatibility and stress-strain relationships as shown below.

Masonry failure:

Assume  $\varepsilon'_m = 0.002$  (optimum masonry compressive strain)

Assume  $\varepsilon_{mu} = 0.0035$  (ultimate masonry compressive strain)

Guess values for  $\alpha$  and  $\beta_1$

Let  $\alpha = 1$  and  $\beta_1 = 1$

Assume the current strain in masonry is at ultimate,

Therefore,  $\varepsilon_m = \varepsilon_{mu} = 0.0035$

The following relations were used to estimate the actual  $\alpha$  and  $\beta$  values:

$$\alpha\beta_1 = \frac{\varepsilon_m}{\varepsilon'_m} + \frac{-1}{3} \left( \frac{\varepsilon_m}{\varepsilon'_m} \right)^2 \quad (\text{Refer to Equation 6.14})$$

$$\alpha\beta_1 \left( 1 - \frac{\beta_1}{2} \right) = \frac{2\varepsilon_m}{3\varepsilon'_m} + \frac{-1}{4} \left( \frac{\varepsilon_m}{\varepsilon'_m} \right)^2 \quad (\text{Refer to Equation 6.15})$$

Therefore,  $\alpha = 0.81$  and  $\beta_1 = 0.9$

Assume,  $k = 0.5$  and  $\varepsilon_f = \varepsilon_{fu} = 0.0273$

These other two relations were used to obtain the actual values of  $k$  and  $\varepsilon_f$

$$\varepsilon_m = \frac{k}{1-k} \varepsilon_f \quad (\text{Refer to Equation 6.16a})$$

$$A_f E_f \varepsilon_f = \alpha\beta_1 k t B f'_{dm} \quad (\text{Refer to Equation 6.17})$$

Therefore,  $k = 0.227$  and  $\varepsilon_f = 0.012$

Calculating the moment in the system:

$$M_n = \alpha\beta_1 k t f'_{dm} \frac{B}{12} \left( t - \frac{\beta_1}{2} k t \right) \quad (\text{Refer to Equation 6.18})$$

$$M_n = (0.81)(0.9)(0.227)(3.625)(1785) \frac{48}{12} \left( 3.625 - \frac{0.9}{2} (0.227)(3.625) \right)$$

$$M_n = 13.952 \text{ k.ft (18.97 kN.m)}$$

$$k_m = \varepsilon_f / \varepsilon_{fu} = 0.012 / 0.027 = 0.44$$

Since  $k_m < 1$ , therefore masonry controlled but still check fiber rupture

Fiber rupture:

$$\alpha\beta_1 = \frac{\varepsilon_m}{\varepsilon'_m} + \frac{-1}{3} \left( \frac{\varepsilon_m}{\varepsilon'_m} \right)^2 \quad (\text{Refer to Equation 6.14})$$

$$\alpha\beta_1 \left( 1 - \frac{\beta_1}{2} \right) = \frac{2\varepsilon_m}{3\varepsilon'_m} + \frac{-1}{4} \left( \frac{\varepsilon_m}{\varepsilon'_m} \right)^2 \quad (\text{Refer to Equation 6.15})$$

$$\varepsilon_m = \frac{k}{1-k} \varepsilon_{fu} \quad (\text{Refer to Equation 6.16a})$$

$$A_f E_f \varepsilon_f = \alpha\beta_1 k t B f'_{dm} \quad (\text{Refer to Equation 6.17})$$

No solution found for  $k$ ,  $\varepsilon_m$ ,  $\alpha$  or  $\beta_1$

Therefore,  $k_m$  still equaled 0.44 and therefore masonry controlled.

Computing Required Shear Resistance: (based on unit inch width of the wall)

Maximum shear force (reaction) in system (Refer to Table B.1.3)

$$\begin{aligned} V_o &= 0.38R_s + 0.12P_{so}L \pm M_n/L \\ &= 0.38(474.83) + 0.12(16.13)(88) \pm (13.952)(1000)(12)/(88)(48) \end{aligned}$$

Therefore, maximum support dynamic reaction,  $V_o = 390.4 \text{ lb}$  (1736.6 N)

Therefore, required shear resistance,  $V_{uo} = 390.4/(88)(1) = 4.44 \text{ psi}$  (30.61 kPa)

Since  $V_{uo} < R_{us}$ , therefore this retrofitted wall has no problem with shear at this blast threat.

Moment at mid-span:

$$\begin{aligned} M_{sp} &= V_d(L/2) - P_{so}(L^2/8) \\ &= [390.4(88/2) - 16.13(88^2/8)] / [(1000)(12)] = 0.16 \text{ k.ft} \text{ (0.22 kN.m)} \end{aligned}$$

Flexural resistance, (Refer to Table B.1.3)

$$R_b = 4(M_n + 2M_{sp})/L = 4(1000)(12)[13.952 + 2(0.16)]/88 = 7785 \text{ lb} \text{ (34.63 kN)}$$

Therefore, flexural unit resistance,  $R_{ub} = 7785/(88)(48) = 1.84 \text{ psi}$  (12.69 kPa)

Since  $R_{ub} < V_{uo}$ , therefore bending controls the wall behavior

Therefore,  $R_u = R_{ub} = 1.84 \text{ psi}$ .

Since  $R_u > R_m$  (0.848 psi), therefore the retrofit provided adequate flexural resistance to the wall.

Checking SDOF Response (for deflection),

Cracked moment of Inertia based on unit width ( $b=1$ ),

$$I_{cr} = bc^3/3 + nA_{fw}(d-c)^2, \text{ where}$$

$$d = t/2 = 3.625/2 = 1.813 \text{ in} \text{ (4.61 cm)}$$

$$n = E_f/E_m = 12000/1606.5 = 7.47$$

$A_{fw}$  = area of FRP/ unit width

$$= \text{area of one sheet} \times b/S = (0.12)(1)/12 = 0.01 \text{ in}^2 \text{ (0.065 cm}^2\text{)}$$

$$c = \frac{-nA_{fw} + \left[ nA_{fw} \left( nA_{fw} + 2bd \right) \right]^{1/2}}{b}$$

$$= \frac{-7.47(0.01) + [7.47(0.01)(7.47(0.01) + 2(1)(1.813))]}{1} = 0.202 \text{ in (0.51 cm)}$$

Therefore,  $I_{cr} = (1)(0.202^3)/3 + 7.47(0.01)(1.813-0.202)^2 = 0.197 \text{ in}^4$

Average moment of Inertia,

$$I_a = (I_g + I_{cr})/2 = [(38/12) + (0.197)]/2 = 1.682 \text{ in}^4$$

Effective Stiffness,

(Refer to Table B.1.3)

$$K_1 = 185E_m I_a / L^3 \text{ (for elastic range)}$$

$$= 185(1606.5)(1.682)/(88^3) = 733.6 \text{ lb/in}$$

$$\Rightarrow 733.6/(88) = 8.33 \text{ psi/in (22.97 kPa/cm)}$$

$$K_2 = 384E_m I_a / 5L^3 \text{ (for plastic range)}$$

$$= 384(1606.5)(1.682)/(5)(88^3) = 304.5 \text{ lb/in}$$

$$\Rightarrow 304.5/(88) = 3.46 \text{ psi/in (9.54 kPa/cm)}$$

Therefore, effective stiffness,  $K = (K_1 + 2 K_2)/2 = 7.63 \text{ psi/in (21.04 kPa/cm)}$

Elastic deflection,

$$y_e = R_u / K_1 = 1.84 / 8.33 = 0.24 \text{ in (0.61cm)}$$

Response in different ranges, average values for  $K_{LM}$  used (Refer to Table B.1.3)

Elastic range:  $K_{M1} = 0.45$ ,  $K_{L1} = 0.58$

$$K_{LM1} = K_{M1}/K_{L1} = 0.45/0.58 = 0.776$$

Elastic-Plastic range:  $K_{M2} = 0.5$ ,  $K_{L2} = 0.64$

$$K_{LM2} = K_{M2}/K_{L2} = 0.5/0.64 = 0.781$$

Plastic range:  $K_{M3} = 0.33$ ,  $K_{L3} = 0.5$

$$K_{LM3} = K_{M3}/K_{L3} = 0.33/0.5 = 0.66$$

$$K_{LM} = (K_{LM1} + K_{LM2} + K_{LM3})/3 = 0.739$$

Equivalent mass (per unit width of wall),

$$M = 597.82 \text{ psi-ms}^2/\text{in} \text{ (1,622.7 kPa-ms}^2/\text{cm)}$$

$$M_e = (K_{LM})(M) = (0.739)(597.82) = 441.8 \text{ psi-ms}^2/\text{in} \text{ (1199.2 kPa-ms}^2/\text{cm)}$$

Natural Period,

$$t_n = 2\pi\sqrt{M_e / K} = 2\pi\sqrt{441.8/7.63} = 47.81 \text{ ms}$$

Duration-Period ratio,

$$\tau = t_d/t_n = 1.83/150 = 0.02$$

Since,  $\tau = 0.038 < 0.1$ , Therefore use Equation 6.9

$$\begin{aligned} \text{Therefore, } \mu_d &= 0.5[(2\pi f I_{so}/R_u)^2 + 1] \\ &= 0.5[(2\pi(1/47.81)(14.77)/1.84)^2 + 1] = 1.056 \end{aligned}$$

Maximum deflection,

$$y_m = (\mu_d)(y_e) = (1.056)(0.24) = 0.255 \text{ in (0.65 cm)}$$

Support rotation,

$$\theta = \tan^{-1}[y_m/(0.5L)] = 0.332 \text{ degree} < 1 \text{ degree (ok)}$$

According to Table B.2.3 (Deformation limit requirements by TM 5-1300), the wall is in a low threat level (below 0.5 degrees) and adequate to resist the specified blast load.

Therefore, the vertical GFRP sheet reinforcement increased the blast capacity of the wall to resist the specified load in a low threat level.

**BIBLIOGRAPHY**

1. Baylot, J. T., Dennis, S. T., and Woodson, S. C., "Response of ¼-Scale Concrete Masonry Unit (CMU) Walls to Blast," Emerging Technologies in Fluids, Structures, and Fluid/Structure Interactions-Volume 1, American Society of Mechanical Engineers (ASME), 2000.
2. Baker, W. E., "Explosion Hazards and Evaluation," Elsevier Scientific Publishing Company, New York, NY, 1983.
3. Biggs, J.D., "Introduction to Structural Dynamics," McGraw-Hill Publishing Company, New York, 1964.
4. "Blast Mitigation for Structures," 1999 Status Report on the DTRA/TSWG Program, The National Academy of Sciences, Washington, D.C, 2000.
5. "Code Requirements for Nuclear Safety Related Concrete Structures (ACI349-40) and Commentary (ACI 349R-90)," ACI Committee 349, American Concrete Institute, Farmington Hills, MI, 1990.
6. "Design of Blast Resistant Buildings in Petrochemical Facilities," prepared by the Task Committee on Blast Resistant Design of Petrochemical Committee of the Energy Division of the ASCE (American Society of Civil Engineers), 1997.
7. Ettouney, M., Smilowitz, R., and Rittenhouse, T., "Blast Resistant Design of Commercial Buildings," Structural Design and Construction, American Society of Civil Engineers (ASCE), 1996.
8. "Structures to Resist the Effects of Accidental Explosions," Departments of the Army, the Navy and the Air Force, Department of the Army Technical Manual



TM 5-1300, Department of the Navy Publication NAVFAC P-397, Department of the Air Force Manual AFM 88-22, November 1990.

9. "Interim Department of Defense Antiterrorism/Force Protection Construction Standards," Department of Defense, 1999.
10. "Masonry Designers' Guide," MDG-3, Third Edition, The Masonry Society, 2001.
11. Masonry Standards Joint Committee, "Building Code Requirements for Masonry Structures," ACI-530-99/ASCE 5-99/TMS 402-99, American Concrete Institute, American Society of Civil Engineers, and The Masonry Society, Detroit, New York, and Boulder, 1999.
12. Muszynski, L. C., "Explosive Field Tests to Evaluate Composite Reinforcement of Concrete and Masonry Walls," Fiber Composites in Infrastructure; Proceedings of the Second International Conference on Composites in Infrastructure, Tucson, Arizona, 1998.
13. Oswald, C. J., and Chang, K. K., "Shock Tube Testing on Masonry Walls Strengthened with Kevlar," to be published.
14. "Protecting Buildings from Bomb Damage-Transfer of Blast Effects Mitigation Technologies from Military to Civilian Applications," The National Academy of Sciences, Washington, D.C, 1995.
15. Tumialan J.G., "Strengthening of Masonry Structures with FRP Composites," Doctoral Dissertation, Department of Civil Engineering, University of Missouri-Rolla, Rolla, Missouri.

16. "Uniform Building Code," International Conference of Building Officials, Whittier, CA, 1994.
17. Whitney, M. G., Oswald, C. J., and Polcyn, M. A., "Blast Damage to Typical Structural Elements," Structures for Enhanced Safety and Physical Security: Proceedings of the Specialty Conference, American Society of Civil Engineers (ASCE), 1989.

